

Role of the dew water on the ground surface in HONO distribution: a case measurement in Melpitz

Yangang Ren¹, Bastian Stieger², Gerald Spindler², Benoit Grosselin¹, Abdelwahid

5 Mellouki^{1*}, Thomas Tuch², Alfred Wiedensohler², Hartmut Herrmann^{2*},

1. Institut de Combustion, Aérothermique, Réactivité et Environnement (ICARE), CNRS (UPR 3021), Observatoire des Sciences de l'Univers en région Centre (OSUC), 1C Avenue de la Recherche Scientifique, 45071 Orléans Cedex 2, France

2. Leibniz Institute for Tropospheric Research (TROPOS), Permoserstraße 15, 04318 Leipzig, 10 Germany

* Corresponding author: Abdelwahid Mellouki (abdelwahid.mellouki@cnrs-orleans.fr) and Hartmut Herrmann (herrmann@tropos.de)

Abstract: To characterize the role of dew water on the ground surface HONO distribution, nitrous acid (HONO) measurements with a MARGA and a LOPAP instrument were performed at the TROPOS research site in Melpitz from April 19th to 29th, 2018. The dew water was also collected and analyzed from May 8th to 14th, 2019 using a glass sampler. The high-time resolution of HONO measurements showed well-defined diurnal variations that revealed: (i) vehicle emission is a minor source of HONO at the Melpitz station; (ii) heterogeneous conversion of NO₂ to HONO on ground surface dominates HONO production at night; (iii) significant nighttime loss of HONO with a sink of 0.16 ± 0.12 ppbv h⁻¹; (iv) dew water with mean NO₂⁻ of 7.91 ± 2.14 µg m⁻² could serve as a temporary HONO source in the morning when the dew droplets evaporate. The nocturnal observations of HONO and NO₂ allowed direct evaluation of the ground uptake coefficients for these species at night: $\gamma_{\text{NO}_2 \rightarrow \text{HONO}} = 2.4 \times 10^{-7}$ to 3.5×10^{-6} , $\gamma_{\text{HONO,ground}} = 1.7 \times 10^{-5}$ to 2.8×10^{-4} . A chemical model demonstrated that HONO deposition to the ground surface at night was 90-100% of the calculated unknown HONO source in the morning. These results suggest that dew water on the ground surface was controlling the temporal HONO distribution rather than straightforward NO₂-HONO conversion. This can strongly enhance the OH reactivity throughout morning time or other planted areas that provide large amount of ground surface based on the OH production rate calculation.

Keywords: HONO, ground surface, NO₂-HONO conversion, dew water, OH production

35 1 Introduction

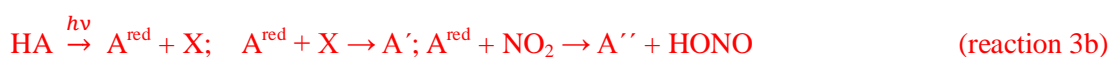
Nitrous acid (HONO) plays an important role in the atmospheric chemistry as its photolysis (reaction 1) is proposed to be an important source of OH radicals. In the troposphere, OH radicals can initiate daytime photochemistry, leading to the formation of ozone (O₃) and secondary organic aerosol (SOA).



At present, the mechanisms of HONO formation have been and are still widely discussed. In the absence of light, heterogeneous reactions of NO₂ occur on wet surfaces (reaction 2) and are considered to be an important source of HONO according to both laboratory studies and field observations (Acker et al., 2004).



Finlayson-Pitts et al. (2003) proposed a mechanism (reaction 2a) involving the formation of the NO₂ dimer (N₂O₄) especially during nighttime. However, this pathway is not important in the real atmosphere (Gustafsson et al., 2008). The surface of soot (Ammann et al., 1998; Arens et al., 2001; Gerecke et al., 1998) or light activated soot (Monge et al., 2010; Aubin and Abbatt, 2007) contain functionalities attached to the large carbonaceous structures or individual condensed organic species, like phenol (reaction 2b) (Gutzwiller et al., 2002) and light-activated humic acids (Stemmler et al., 2006), which undergo electron transfer reactions with NO₂ yielding HONO (reaction 3b). This reaction is also postulated for aromatics in the aqueous phase, but only proceeds at a relevant rate at high pH levels (Ammann et al., 2005; Lahoutifard et al., 2002). Gustafsson et al. (2008) provide the evidence that formation of HONO proceeds by a bimolecular reaction of absorbed NO₂ and H (reaction 4) on mineral dust, where H formed from the dissociation of chemisorbed water. However, Finlayson-Pitts (2009) indicated that this pathway is probably not transferable from laboratory to real atmosphere. In addition to the direct emission from the vehicle exhaust (Kurtenbach et al., 2001) and homogeneous gas phase reaction of NO with OH (reaction 3a) (Pagsberg et al., 1997), some other HONO formation mechanisms have been proposed e.g. homogeneous nucleation of NO₂, H₂O, and NH₃ (reaction 5) (Zhang and Tao, 2010); photolysis of nitric acid and nitrate (HNO₃/NO₃⁻) (reaction 6) (Ye et al., 2016; Zhou et al., 2011) and nitrite emission from soil (reaction 7) (Su et al., 2011). However, the dominant HONO formation mechanism is still under discussion.





Several studies (He et al., 2006;Rubio et al., 2009;Acker et al., 2004;VandenBoer et al.,
75 2013;Lammel and Cape, 1996;Lammel and Perner, 1988;VandenBoer et al., 2014) reported
that deposited HONO on wet surfaces can be a source for observed daytime HONO. Few of
them have simultaneously quantified both dew and atmospheric composition. He et al. (2006)
observed HONO released from a drying forest canopy and their lab studies show that, on
average, ~90% of NO_2^- was emitted as HONO during dew evaporation. Rubio et al. (2009)
80 found a positive correlation between formaldehyde and HONO in dew and the atmosphere.

The dominant loss of HONO is photolysis during daytime, which forms OH radicals
according to **reaction 1**. An additional sink of HONO is the reaction with OH radical (**reaction
9**). Due to the absence of solar radiation and the low OH concentration, the main loss process
of HONO during nighttime is dry deposition, which can reach the balance with HONO
85 production and vertical mixing to generate a steady state of HONO **mixing ratio**.



Due to its significant atmospheric importance, HONO has been measured for many years
with various techniques (Platt et al., 1980;Kanda and Taira, 1990;Febo et al., 1993;Wang and
Zhang, 2000;Schiller et al., 2001;Huang et al., 2002). **Long Path Absorption Photometer
90 (LOPAP)** is a two channel in situ HONO measurement instrument, which **detects** HONO
continuously by wet sampling and photometric detection. LOPAP is very selective without
sampling artefact and chemical interferences (e.g. NO_2 , NO , O_3 , HCHO , HNO_3 , SO_2 and PAN
etc.). In addition, the detection limit of LOPAP can go down to **0.2 pptv** (Kleffmann and
Wiesen, 2008) by optimizing the parameters like (a) sample gas flow rate, (b) liquid flow
95 rates, and (c) the length of the absorption tubing (Heland et al., 2001). LOPAP was validated
and compared with the most established and reliable HONO instrument **Differential Optical
Absorption Spectroscopy (DOAS)**, both **used** in the field and a large simulation chamber
under various conditions, and found excellent agreement (Heland et al., 2001;Kleffmann et al.,
2006). **Monitor for AeRosols and Gases in ambient Air (MARGA)** is a commercial instrument
100 combining a Steam-Jet Aerosol Collector (SJAC) and a Wet Rotating Denuder (WRD), which
can quantify the inorganic water-soluble PM ions (Cl^- , NO_3^- , SO_4^{2-} , NH_4^+ , Na^+ , K^+ , Mg^{2+} , Ca^{2+})
and corresponding trace gases (HCl , HONO, HNO_3 , SO_2 , NH_3). In recent years, MARGA
measurements were performed worldwide, which has been summarized by Stieger et al.
(2018). **The cited group found a large scattering ($R^2 = 0.41$) for the HONO comparison
105 between MARGA and an off-line batch denuder without an inlet system. The probable reason
was the off-line analysis of the batch denuder sample as the resulting longer interaction of gas
and liquid phase during the transport led to further heterogenous reactions. Hence, that**

induces an interesting objective of inter-comparison between MARGA and LOPAP for HONO measurements.

110 In this study, we present parallel measurements of HONO using LOPAP and MARGA in Melpitz, Germany, over two weeks in 2018. For further investigations, dew water was collected and analyzed from May 8th to 14th 2019 using two glass samplers. In addition, other water-soluble compounds, such as gaseous HNO₃, NH₃ and particulate NO₃⁻, SO₄²⁻, NH₄⁺, Na⁺, K⁺, Mg²⁺, Ca²⁺, trace gases (NO_x, SO₂ and O₃) and meteorological parameters were also
115 measured simultaneously. Our observations provide a direct inter-comparison between LOPAP and MARGA for HONO field measurement, additional insights into HONO chemical formation processes and examine the relative importance of the HONO source.

2 Experimental

2.1 Site description

120 Measurements were performed at the research station of the Leibniz Institute for Tropospheric Research (TROPOS) in Melpitz (12°56'E, 51°32'N). This rural field site is situated on a meadow and surrounded by flat grass land, agricultural areas and forests. The Melpitz site mainly can be influenced by two different wind direction: west wind origin from the marine crossing a large area of Western Europe and the city of Leipzig (41 km NE), and east wind
125 crossing Eastern Europe (Spindler et al., 2004).

2.2 MARGA instrument

The MARGA (1S ADI 2080, The Netherlands) was used in this study and has already been described in Stieger et al. (2018), so only short information is provided here. An inlet flow of
130 1 m³ hr⁻¹ was drawn into the sampling box after passing through an inside Teflon-coated PM₁₀ inlet (URG, Chapel Hill, 3.5 m). Within the sample box, the sampled air laminarly passed a WRD in which water-soluble gases diffuse into a 10 mg l⁻¹ hydrogen peroxide (H₂O₂) solution at pH = 5.7. Particles can reach the SJAC because of their smaller diffusion velocities. Within the SJAC, the particles grow into droplets under supersaturated water vapor conditions and were collected by a cyclone. Then, the aqueous samples of the WRD (gas phase) and the
135 SJAC (particle phase) were successively injected into two ion-chromatographs (IC) with conductivity detectors (Metrohm, Switzerland) by two syringe pumps (25 ml) for analyzing the anions and cations. The Metrosep A Supp 10 (75/4.0) column and Metrosep C4 (100/4.0) column were used to separate anions and cations, respectively. Lithium bromide was used as the internal standard for both gas- and particle-phase samples added during the sample
140 injection to the IC. The gas and particle samples are both collected over the course of one hour.

The detection limit of the HONO measurements with the MARGA system is 0.02 µg m⁻³

(Stieger et al., 2018). We performed blank measurements for the MARGA before the intercomparison campaign in 2018. For this, the MARGA was set to the blank measurement mode that has a duration of six hours. Within the first 4 hours, the MARGA air pump was off and the denuder and SJAC liquids were analyzed. The first- and second-hour samples are discarded as they still include residual concentrations. The evaluation of the blank concentrations was performed for the third- and fourth-hour samples. Within these blank samples, $0.00 \mu\text{g l}^{-1}$ of nitrite both in the gas and particle phase were measured indicating no background nitrite collection.

2.3 LOPAP instrument

The LOPAP (QUMA, Germany) employed in this work was described in previous studies (Bernard et al., 2016; Heland et al., 2001). Only brief description is given here. The LOPAP instrument consists of two sections: a sampling unit and a detection unit. The ambient air was sampled in the sampling unit, which composed of two glass coils in series where the first coil (channel 1) accounted for HONO with interferences and the second coil (channel 2) only interferences assuming that more than 99 % of HONO was absorbed into acidic stripping solution (R1) to form diazonium salt in channel 1. This salt reacts with solution R2 (0.8mM n-(1-naphthyl)ethylenediamine-dihydrochloride) to produce final azo dye, which is photometrically detected by long path absorption in a special Teflon tubing (Kleffmann et al., 2006; Heland et al., 2001). During our field campaign in Melpitz, the temperature of the stripping coil was kept constant at $25 \text{ }^{\circ}\text{C}$ by a thermostat. Automatic zero air (Air liquid, Alphagaz 2, 99.9999%) measurements were performed for 30 min per 12 h measurements to correct for zero drifts. In addition, three calibrations using NO_2^- standard solution (Heland et al., 2001) were applied in the beginning, middle and end of the campaign, to derive the HONO mixing ratio of our field campaign with a detection limit of LOPAP as 0.6 pptv, and then the error of HONO mixing ratio was estimated based on the detection limit and a relative error as 10%.

To investigate the possible sampling inlet and denuder artefacts of the MARGA, two different positions were settled for LOPAP during the measurement period (explained in SI): M1, sampling unit of LOPAP was connected to the MARGA inlet in the back of the 2 m sampling tube and the PM_{10} inlet of MARGA as shown in Figure S1a (April 18th, 2018 13:00 UTC –April 20th, 2018 08:00 UTC); M2 the sampling unit of LOPAP was settled in the same level as the sampling head of MARGA (Figure S1b) (April 20th, 2018 15:00 UTC –April 29th, 2018 07:00 UTC).

2.4 Dew water collection and analysis

To evaluate the HONO emission from the dew water in the morning, the dew water was

collected and analyzed one year later on May 8th, 11th, 13th and 14th 2019. Similar conditions (grass height, dew formation and day length) were observed to improve the evaluation. For dew sampling, a glass sampler was used (as shown in Figure S2). Two 1.5 m² glass plates (Plate 1 and Plate 2) were placed 40 cm above the ground with a tilt angle of approximately 10°. A gutter was installed at the lower end of each plates to collect the running down water. The water is trapped in 500 ml bottles. The dew samplers were prepared each evening before a likely dew event occurred (low dew point difference, clear sky and low winds). Each plate was rinsed with at least 2 L ultrapure water. A squeegee removed the excess water. Afterwards, the plates were cleaned with ethanol and were again rinsed by 2 L ultrapure water. The plate was splashed with ultrapure water and squeegeed six times and the gutter was cleaned. The sample of the sixth splash was collected as blank.

The dew water normally was collected from 18:00 to 5:00 (UTC). In the morning, the excess dew on the plate was squeegeed. To achieve the volume of dew (V_{dew}), the bottles were weighted before and after sampling by a balance. The pH was measured by a pH meter (mod. Lab 850, Schott Instruments) on a subsample of the total volume. After sampling, the aqueous solutions were filtered and stored in a fridge (~6 °C). Within six hours, the HONO analyses of the dew and blank samples were performed by double-injection in the MARGA in the manual measurement mode as HONO may volatilize between sampling and analysis. For the other ions (Cl⁻, NO₃⁻, SO₄²⁻, Oxalate, Br⁻, F⁻, Formate, MSA, PO₄³⁻, Na⁺, NH₄⁺, K⁺ and Mg²⁺, Ca²⁺), the samples were analyzed with laboratory ion chromatogram systems (mod. ICS-3000, Dionex, USA). Blanks from water, the filter, the syringes and bottles were subtracted.

2.5 Aerosol measurements

The particle size distributions were measured in the size range from 5 nm to 10 µm employing by a Dual Mobility Particle Size Spectrometer (TROPOS-type D-MPSS) (Birmili et al., 1999) and an Aerodynamic Particle Size Spectrometer (APSS model 3321, TSI Inc., Shoreview, MN, USA). For the particle number size distribution measurements, the aerosol is sampled through a low flow PM10 inlet and dried in an automatic diffusion dryer (Tuch et al., 2009). The measurements and quality assurance are done following the recommendations given in Wiedensohler et al. (2012) and Wiedensohler et al. (2018). The MPSS derived particle number size distribution was inverted by the algorithm described in Pfeifer et al. (2014), following the bipolar charge distribution of Wiedensohler (1988).

2.6 Other measurements

Trace gases of NO-NO₂-NO_x, SO₂ and O₃ were measured by NO_x analyzer (Thermo Model 42i-TL, Waltham, Massachusetts, USA), SO₂ analyzer APSA-360A and O₃ analyzer APOA 350 E (both Horiba, Kyoto, Japan) with a time resolutions of 1 min. It should be noted that

NO₂ was converted to NO within the NO_x analyzer by a blue light converter BLC2 (Meteorologie Consult GmbH, Königstein, Germany). The provider for replacement of the Mo-Converter in the 42i-TL analyzer is MLU Messtechnik GmbH, Essen Germany. Meteorological parameters like temperature (T), precipitation, relative humidity (RH) as well as wind velocity and direction were measured by PT1000, a rain gauge (R.M. Young Company, U.S.A.), the CS215 sensor (SensirionAG, Switzerland) and a WindSonic by Gill Instruments (UK), respectively. Global radiation and barometric pressure were recorded by a net radiometer CNR1 (Kipp&Zonen, The Netherlands) and a digital barometer (Vaisala, Germany), respectively.

2.7 Calculation of photolysis rate

Off-line NCAR Tropospheric Ultraviolet and Visible (TUV) transfer model (<https://www2.acom.ucar.edu/modeling/tropospheric-ultraviolet-and-visible-tuv-radiation-model>) was used to estimate the photolysis rate of HONO (J_{HONO}), NO₂ (J_{NO_2}) and production rate of O¹D ($J_{\text{O}^1\text{D}}$) at the Melpitz station. Aerosol optical depth (AOD), total vertical ozone column, total NO₂ column, total cloud optical depth and surface reflectivity (Albedo) were taken from the NASA webpage for the period of measurement (<https://neo.sci.gsfc.nasa.gov/blog/>).

3 Results

3.1 Inter-comparison of LOPAP and MARGA

The hourly HONO mixing ratio obtained from MARGA is compared with the 30 seconds and hourly averaged HONO mixing ratios from LOPAP, respectively, as shown in Figure 1a and 1b. It indicates that the MARGA values were higher than the values of LOPAP but not during the peak events. The comparisons of the MARGA and LOPAP HONO measurements for period M1 and period M2 in Figure 1c result in slopes of 1.58 and 1.90 using Deming regression, respectively. The result is in excellent agreement with the former intercomparison of both instrument types in the Chinese field campaign (Lu et al., 2010; Xu et al., 2019) where the HONO mixing ratio measured with the wet-denuder-ion-chromatography (WD/IC) instrument was affected by a factor of three on average.

Recently, Stieger et al. (2018) evaluated the HONO measurement of the on-line MARGA system with another off-line batch denuder setup. The correlation was weak and the scatter large that is in agreement with the literature (Acker et al., 2004; Genfa et al., 2003). The off-line batch denuder is similar to the MARGA WRD and consists of a rotating annular denuder in an open system without inlet tubes to avoid interactions of sampled air and walls. The liquid is collected after sampling for one hour and is analyzed off-line with ion chromatography (Stieger et al. 2018). Genfa et al. (2003) reported that they found a

discrepancy between two denuder systems working with Na_2CO_3 and H_2O_2 resulting in different pH. However, in the comparison by Stieger et al. (2018), the MARGA system and the off-line batch denuder had the same pH and the found differences (scattering) cannot be explained by pH differences. More likely is the different analysis time after sampling regarding on-line MARGA compared to off-line batch denuder. The evaporation of solved HONO from the off-line sample and heterogeneous reactions of NO_2 and H_2O as well as NO_2 and SO_2 in water described by Spindler et al. (2003) or VOCs by NO_2 could explain the artefacts in the denuder solution (Kleffmann and Wiesen, 2008), which could account for ca. 58% (M1, where both LOPAP and MARGA used the common MARGA inlet) of these ca. 90% of overestimated HONO measurement from MARGA. Additional artefacts as heterogeneous formation of HONO due to the long MARGA inlet system should be responsible for another ca. 32% (the difference between slopes M2 and M1). Hence, the results show that the use of massive sampling inlets, even if they are coated by Teflon, should be avoided for any in-situ HONO instrument. As a result, we chose the LOPAP-measured HONO in the following sections because of its high precision.

3.2 General results

Figure 2 and Figure 3 show an overview of the measured HONO, NO, NO_2 , O_3 , $\text{PM}_{1.0}$, $\text{PM}_{2.5}$, PM_{10} , meteorological parameters, water-soluble ions in PM_{10} (NO_3^- , SO_4^{2-} , NH_4^+ , Na^+ , K^+ , Mg^{2+} , Ca^{2+}) and their corresponding trace gases (HONO, HNO_3 , SO_2 , NH_3) in the present study. The daytime (D, 04:00-18:00, UTC) and nighttime (N, 18:00-04:00) averages are also provided in Table 1. During the two weeks measurement, the prevailing winds were from the southwest and northwest sectors, indicating a possible influence of city emission from Leipzig, Germany, on the site. However, the strong wind (maximum 13 m s^{-1}) led to a low PM concentration with low concentration of water-soluble ions in PM_{10} (NO_3^- , SO_4^{2-} , NH_4^+) and their corresponding trace gases (HNO_3 , SO_2 , NH_3) during the period April 24th to 29th, 2018. The air temperature ranged from 5 °C to 27 °C and the RH showed a clear variation pattern with higher levels during the night and lower levels during daytime. During the campaign, good air quality was observed with daily averaged $\text{PM}_{2.5}$ concentration of $15 \pm 4 \mu\text{g m}^{-3}$. In addition, low mixing ratio of NO and NO_2 with a diurnal average of 0.9 ± 1.2 ppbv and 3.7 ± 2.2 ppbv, respectively, were recorded. These observations highlight the nature of our measurement site as a typical background environment. The HONO concentration from the LOPAP measurements varied from 30 pptv to 1582 pptv and showed diurnal variations (with an average of 162 ± 96 pptv and 254 ± 114 pptv during daytime and nighttime, respectively) except for two sets of observations, which will be discussed in the following section.

Größ et al. (2018) reported the linear function of the global radiation flux vs. OH radical concentration for the campaign EUCAARI 2008 at Melpitz.

$$[\text{OH}] = A * \text{Rad} \quad (\text{Eq. 1})$$

285 with Rad being global solar irradiance in W m^{-2} and [OH] is the hydroxyl radical concentration. The proportionality parameter A is $6110 \text{ m}^2 \text{ W}^{-1} \text{ cm}^{-3}$. On the basis of such a correlation, we derived the OH concentration during the period of this field measurement, with an average of $(2.8 \pm 0.7) \times 10^6$ during daytime.

3.3 Diurnal variation of HONO, particles and trace gas species

290 The diurnal profiles of HONO and related supporting parameters are shown in Figure 4 for the whole period except for **two sets of observations**: (1) no HONO peak in the morning of April 23rd and (2) HONO peak observed at 0:00-2:00 (UTC) of April 25th (Figure 5). Overall, the HONO increased fast after the sunrise and peaked at 7:00 (UTC), which then dropped rapidly and reached a minimum at around 10:00 (UTC) and kept until 17:00 (UTC). **As shown**

295 **in Figure 4a, 4e and 4f, the diurnal variation trend of HONO during daytime was similar to the one of NH_3 in the gas phase as well as NO_3^- and NH_4^+ in PM_{10} . This induced the hypothesis (a) of HONO morning peak might possibly be caused by the photolysis of particle-phase $\text{HNO}_3/\text{NO}_3^-$ (Zhou et al., 2003; Ye et al., 2016; Zhou et al., 2011). This morning peak of HONO has been reported for Melpitz (April 4th-14th, 2008) by Acker et al. (2004),**

300 **who expected that the storage of HONO on wet surfaces can be a source for observed daytime HONO. Such daytime pattern was also found in Spain, for a site surround by forests and sandy soils (Sörgel et al., 2011). Sörgel et al. (2011) explained this by local emissions, which are trapped in the stable boundary layer before its breakup of the inversion in the morning based on a similar diurnal cycle for NO and NO_2 , which is different with this work. In this**

305 **work, the NO_2 mixing ratio decreased from the midnight until noon and NO peaked at 5:00 (UTC) then kept low concentration (<1 ppbv) for 18 hours of one day. However, the photosensitized NO_2 on humic acid could act as a source of HONO during the daytime as reported by Stemmler et al. (2006) then which might lead to a HONO morning peak within hypothesis (b). For hypothesis (c), it was observed that dew was formed overnight during our**

310 **campaign in Melpitz. Gaseous HONO could be deposited in these droplets. Due to evaporation after sunrise, HONO would be reemitted in the atmosphere and led to a HONO morning peak. These hypotheses will be further discussed in Section 4.**

As shown in Figure 4a and 4b, the HONO and NO_2 concentrations started to increase coincidentally at 16:00 (UTC) when the sunshine was weak. This **is** explained by the

315 heterogeneous conversion of NO_2 to HONO during nighttime and will be discussed in Section 4. However, the HONO **mixing ratio** then decreased from 21:00 (UTC) to around 100 pptv even though the NO_2 concentration kept constant around 5-6 ppbv. This decrease during nighttime indicates the HONO loss process (dry and wet deposition, trapped in the boundary layer or dew etc.) surpassing **the HONO formation from the NO_2 -to-HONO conversion**. The

320 diurnal cycle of O₃ reflects the balance between the photochemical formation of O₃ (e.g. NO₂ + hv) and O₃ consumption (e.g. ozonolysis of terpenes).

3.4 HONO in the dew water

Dew water formation on canopy surfaces could be an efficient removal pathway of water soluble pollutants. High solubility of HONO makes dew water an efficient sink and a stable
325 reservoir for atmospheric HONO. Actually, a lot of dew water has been observed on the grass around the Melpitz station during the sampling period of April 19th to 29th, 2018. Hence, to investigate the dissolved HONO in the dew water of Melpitz station, the dew water was collected and analyzed from May 8th to 14th 2019 at the same season like the HONO measurements. Many ions e.g. NO₂⁻, Cl⁻, NO₃⁻, SO₄²⁻, Oxalate, Br⁻, F⁻, Formate, MSA, PO₄³⁻,
330 Na⁺, NH₄⁺, K⁺ and Mg²⁺, Ca²⁺ were analyzed using MARGA and laboratory IC, but our discussion only focuses on NO₂⁻. The sample parameters (time, pH etc.) and NO₂⁻ concentration in the sample (μg L⁻¹) are shown in Table 2 from two glass plates (plate 1 and plate 2). The final dew water NO₂⁻ was calculated by subtracting the blank NO₂⁻ from the raw data of dew water analysis in MARGA. The pH of dew water in Melpitz ranged from 6.30 to
335 7.00. It should be noted that the dew water was frozen until 1 hour after sunrise on May 8th, 13th and 14th 2019 but not on May 11th 2019. At this day, a third sample was collected sampled from 3:30 to 5:20 (UTC) after collecting the first sample (18:00-3:20 UTC). The NO₂⁻ concentration per m² of the sampler surface (F_{NO2-}) was calculated from the following equation:

$$340 \quad F_{\text{NO}_2^-} = \frac{[\text{NO}_2^-] \times V_{\text{dew}}}{1.5 \text{m}^2 \times 1000} \quad (\text{Eq. 2})$$

Where [NO₂⁻] is the sample concentration in μg L⁻¹, V_{dew} is the sample volume in ml, 1.5 m² is the surface area of the glass sampler. As shown in Table 2, higher F_{NO2-} was obtained on May 11th where dew water was not frozen. On other days (May 8th, May 13th and May 14th) frozen dew water was observed, which likely inhibited HONO to dissolve. Hence, these frozen
345 samples were not considered in this paper. On May 11th, the final F_{NO2-} could be obtained by averaging F_{NO2-} of the sum (9.43 μg m⁻²) of the first and third sample with the second sample (6.40 μg m⁻²) on 11th May resulting in 7.91 ± 2.14 μg m⁻². This value will be used for the following calculation and discussion.

4 Discussion

350 4.1 Contribution of vehicle emissions

Since Melpitz site is close to a main national road from Leipzig to Torgau (Germany) that is within the main southwest wind direction, the contribution of vehicle emissions to the measured HONO mixing ratio should be evaluated. Generally, the HONO/NO_x ratio is usually

chosen to derive the emission factor of HONO in the freshly emitted plumes (Kurtenbach et al., 2001). As illustrated in Figure S3, NO_x concentrations were normally lower than 15 ppbv and NO/NO_x ratios were ~0.4 in this campaign, suggesting the detected air is a mixture of fresh and aged air during the measurement period. Therefore, a substantial part of HONO is secondary. Additionally, following the criteria of Li et al. (2018), the bad correlation between HONO and NO_x ($R^2 \approx 0.35$) suggests that the direct HONO emission from the vehicle emitted plumes were less important in this work.

4.2 Nighttime HONO

The nighttime HONO is different to some reported literatures (Li et al., 2012; Zhou et al., 2007; Huang et al., 2017; Wang et al., 2017). HONO increased after sunset to a maximum at 21:00 (UTC) and decreased until sunrise.

4.2.1 Formation through heterogeneous conversion of NO₂

The ratio of [HONO]/[NO₂] is generally used as an index to estimate the efficiency of heterogeneous NO₂-HONO conversion because it is less influenced by transport processes than individual concentrations. However, the ratio might be influenced when a large fraction of HONO is emitted from the traffic but this is expected to be less important as shown in section 4.1. However, a low emission factor of 0.3% was used to correct the directly HONO emission from the NO₂-HONO conversion (Kurtenbach et al., 2001). Six conditions as listed in Table 3 are selected to calculate the NO₂-HONO frequency following the criteria of Li et al. (2018):

- (a) only the nighttime data in the absence of sunlight (i.e., 17:30-06:00 UTC) are used;
- (b) both HONO mixing ratio and [HONO]/[NO₂] ratios increased steadily during the target case;
- (c) the meteorological conditions, especially surface winds, should be stable.

Figure S4 presents an example of the heterogeneous HONO formation occurring on April 28th, 2018. In this case, the HONO mixing ratios increased rapidly after sunset from 100 pptv to 600 pptv. Together with the HONO mixing ratio, the [HONO]/[NO₂] ratio increased almost linearly between 18:00 to 19:50 UTC. The slope fitted by the least linear regression for [HONO]/[NO₂] ratios against time can be taken as the conversion frequency of NO₂-to-HONO (k_{het}).

The ratio of [HONO]/[NO₂] during the Melpitz campaign ranged from 0.055 (5.5%) to 0.161 (16.3%) with mean value of 0.110 ± 0.041 (Table 3) using the data during early nighttime (17:30-00:00 UTC). This mean values are within the wide range of reported values 0.008-0.13 in the fresh air masses from the most sampling sites (Alicke et al., 2002; Alicke et al., 2003; Zhou et al., 2007; Su et al., 2008; Sörgel et al., 2011; Wang et al., 2017; VandenBoer et

al., 2013) except for the study of Yu et al. (2009), who got a high value as 0.3. However, to
390 our best knowledge, this work presents also a high NO₂-to-HONO conversion frequency k_{het}
of $0.027 \pm 0.017 \text{ h}^{-1}$ compared with most of the previous studies at urban sites, such as Wang et
al. (2013) in Shanghai (0.007 h^{-1}), Alicke et al. (2002) in Milan (0.014 h^{-1}), Wang et al. (2017)
in Beijing (0.008 h^{-1}) and Huang et al. (2017) in Xi'an (0.0091 h^{-1}). However, our value is
395 h^{-1} , who also conducted rural measurements in the Pearl River Delta (PRD) area in Southern
China and in Pabstthum, Germany, respectively, surrounded by farmland (grasses, trees, small
forests). This could be ascribed to the higher S/V surface in the rural site because of the high
leaf area index (LAI, m^2/m^2) compared to an urban and might have enhanced the
heterogeneous NO₂-HONO conversion.

400 4.2.2 Relative importance of particle and ground surface in nocturnal HONO production

The particle surface density S_a was calculated from the particle size distribution (Figure S5)
ranged from 5 nm to 10 μm of APSS and D-MPSS data by assuming the particle are in
spherical shape. The particle surface density S_a was further corrected with a hygroscopic
405 factor $f(\text{RH})=1+a \times (\text{RH}/100)^b$ (empirical factors a and b were set to 2.06 and 3.6, respectively)
following the method of Li et al. (2012) and Liu et al. (2008).

The formation of HONO through heterogeneous NO₂ conversion on particle surfaces (S_a)
can be approximated following the recommendations in Li et al. (2010):

$$k_{\text{het}} = \frac{1}{4} \gamma_{\text{NO}_2 \rightarrow \text{HONO}_a} \times v_{\text{NO}_2} \times \frac{S_a}{V} \quad (\text{Eq.3})$$

410 where v_{NO_2} is the mean molecular velocity of NO₂ (370 m s^{-1}) (Ammann et al., 1998); S_a/V is
the particle surface to volume ratio (m^{-1}) representing the surfaces available for heterogeneous
reaction, and $\gamma_{\text{NO}_2 \rightarrow \text{HONO}_a}$ is the uptake coefficient of NO₂ at the particle surface. If the entire
HONO formation was taking place on the particle surface, the calculated $\gamma_{\text{NO}_2 \rightarrow \text{HONO}_a}$ varied
415 from 1.5×10^{-6} to 1.9×10^{-5} with a mean value of $(8.8 \pm 5.0) \times 10^{-6}$, which is lower than the
reported values from VandenBoer et al. (2013) as 10^{-4} but it is in the good agreement with
those observed in studies on relevant surfaces, which ranged between 1×10^{-6} to 1×10^{-5}
(Kleffmann et al., 1998;Kurtenbach et al., 2001). Moreover, given the weakened correlation
between HONO ($R^2=0.566$), $[\text{HONO}]/[\text{NO}_2]$ ($R^2=0.208$) and S_a (Figure S6), this work
concludes that, as previously reported (Wong et al., 2011;Sörgel et al., 2011;Kalberer et al.,
420 1999), the HONO formation through heterogeneous NO₂ conversion on particle surfaces
needs to be regarded as unimportant.

As illustrated above, the heterogeneous NO₂ conversion on ground surfaces (including
surfaces such as plants, building, soils etc.) contributes mainly to nighttime formation of

HONO, which can be approximated by Eq.4 following the method in literatures (Li et al.,
425 2010;Kurtenbach et al., 2001;VandenBoer et al., 2013;VandenBoer et al., 2014) and also been
applied by Zhang et al. (2016):

$$k_{\text{het}} = \frac{1}{8} \gamma_{\text{NO}_2 \rightarrow \text{HONO}_g} \times v_{\text{NO}_2} \times \frac{S_g}{V} \quad (\text{Eq.4})$$

where $\gamma_{\text{NO}_2 \rightarrow \text{HONO}_g}$ is the uptake coefficient of NO_2 at the ground surface, S_g/V represents the
ground surface to volume ratio. As described by Zhang et al. (2016), the LAI was used to
430 estimate the surface to volume ratio for the vegetation-covered areas, following the method in
Sarwar et al. (2008):

$$\frac{S_g}{V} = \frac{2 \times \text{LAI}}{H} \quad (\text{Eq.5})$$

Where H is the mixing layer height, which was calculated from the backward trajectory
based on GDAS data and a range of 20 m to 300 m from 17:00 until around 00:00 UTC in
435 April 2018 was used in present study (Figure S7). The LAI value is multiplied by a factor of 2
to take the areas on both sides of the leaves into account and is around 4 to 10 for grassland
values. In Wohlfahrt et al. (2001), the LAI for meadows with different heights are given.
Regarding the height (~30 cm) in April 2018, we used a factor of 6 in present study. If the
entire HONO formation was taking place on the ground surface, the calculated $\gamma_{\text{NO}_2 \rightarrow \text{HONO}_g}$
440 varied from 2.4×10^{-7} to 3.5×10^{-6} with a mean value of $2.3 \pm 1.9 \times 10^{-6}$. This value agrees well
with the reported range of $\gamma_{\text{NO}_2 \rightarrow \text{HONO}}$ from 10^{-6} to 10^{-5} on the ground surface based on the
laboratory studies (Donaldson et al., 2014;VandenBoer et al., 2015) and field campaign in
Colorado, USA (VandenBoer et al., 2013) during the night time. However, it should be noted
that the obtained NO_2 uptake coefficient on the ground surface is closely to the reactive
445 surface provided by aerosols, but as the S/V ratio of particles is typically orders of magnitude
lower than for ground surfaces, it is suggested that the heterogeneous reactions of NO_2 on
ground surface may play a dominant role for the nighttime HONO formation.

4.2.3 HONO deposition on the ground surface

As illustrated in Figure 4a and S4, between midnight and sunrise (22:00-4:00 UTC), the
450 deposition of HONO becomes increasingly important as the absolute amount of HONO
decreased. Assuming a constant conversion frequency of NO_2 -to-HONO, k_{het} , the HONO
deposition rate (L_{HONO}) can be roughly estimated by:

$$L_{\text{HONO}} = \frac{d[\text{HONO}]}{dt} - k_{\text{het}} \times [\text{NO}_2] \quad (\text{Eq. 6})$$

The strength of the HONO sink during night is average 0.16 ± 0.12 ppbv h^{-1} and ranged from
455 0.041 to 0.447 ppbv h^{-1} , and this value is similar with reported ones in the literature (He et al.,
2006).

The relationship of $[\text{HONO}]/[\text{NO}_2]$ with RH during nighttime (18:00-04:00) is illustrated

in Figure S8a. A positive trend of [HONO]/[NO₂] ratio along the RH was found when RH was less than 70%, however, [HONO]/[NO₂] performs a negative trend with RH for values over 460 70%. The same phenomenon was also observed by Yu et al. (2009) in Kathmandu and Li et al. (2012) in PRD region, China. This finding can be associated with larger amounts of dew water on various ground surfaces (plants and grasses) when ambient humidity approached saturation, leading to an efficient uptake of HONO. The relationship of NO₂-HONO conversion frequency (k_{het}) with the inverse of wind speed during nighttime (18:00-04:00) is 465 illustrated in Figure S8b. As indicated in Figure S8b, wind speed was predominantly less than 3 m s⁻¹ during the field campaign period in Melpitz and high conversion frequency of NO₂-to-HONO mostly happened when wind speed was less than 1 m s⁻¹. However, one point showed highest NO₂-HONO conversion frequency (k_{het}) happened when wind speed was ca. 4 m s⁻¹ according to the second set of observation mentioned in section 3.3 and Figure 5, mainly 470 due to the evaporation of dew droplets resulting in the temporary HONO peak. Additionally, these samples indicate that the wind speed would also influence HONO deposition on the ground surface through decreasing RH (discussion in the following Section 4.3).

Assuming all the extra HONO were removed through deposition on the ground surface, the change of HONO in the time interval of 22:00-04:00 (UTC) is parameterized using a 475 combination of Eq. 8 and the following equation:

$$L_{\text{HONO}} = \frac{1}{4} \gamma_{\text{HONO,ground}} \times [\text{HONO}] \times \frac{v_{\text{HONO,ground}}}{H} \quad (\text{Eq. 7})$$

Where $\gamma_{\text{HONO,ground}}$ is the HONO uptake coefficient on the ground surface, $v_{\text{HONO,ground}}$ is the mean molecular velocity of HONO and $3.67 \times 10^4 \text{ cm s}^{-1}$ was used, H is the mixing layer height calculated from the backward trajectory based on GDAS data ranging between 20 m 480 and 150 m with an average of ca. 55 m from 22:00 until 04:00 UTC in April 2018. This approach yielded to a $\gamma_{\text{HONO,ground}}$ uptake coefficient in the range of 1.7×10^{-5} to 2.8×10^{-4} with average of $(1.0 \pm 0.4) \times 10^{-4}$, which is similar as the data found in Boulder, Colorado, ranging from 2×10^{-5} to 2×10^{-4} (VandenBoer et al., 2013).

However, as observed by several studies (He et al., 2006; Rubio et al., 2009; Wentworth et al., 485 2016), the effective Henry's law solubility of HONO is highly pH-dependent (from borderline soluble at pH = 3 to highly soluble at pH \geq 6), as would be expected for a weak acid. The Melpitz station is surrounded by grass land and tilled earth, the pH of collected dew water during nighttime in May 2019 was 6.3-7.0 (Table 2), where the effective Henry's law solubility of HONO would be high. Furthermore, the amount of HONO in this dew water was 490 quantified using MARGA and ranged between 41.87 and 164.62 mg L⁻¹, which is higher than NO₂⁻ in Santiago's dew waters (Rubio et al., 2009). This could strongly support the obtained HONO uptake coefficient on the ground surface. These field-derived surface parameters of nighttime HONO production from NO₂ and surface deposition of HONO are valuable to the

model evaluation.

495 A simple resistance model based on the concept of aerodynamic transport, molecular diffusion and uptake at the surface (presented in SI) as proposed by Huff and Abbatt (2002) was used to evaluate the factor(s) controlling the potential applicability of the γ -coefficients calculated here for the uptake of NO_2 and deposition of HONO. As shown in Figure S9, the deposition loss of HONO is potentially limited by a combination of aerodynamic transport, molecular
500 diffusion and reaction processes. However, the HONO uptake will be transport-limited if the real uptake coefficients are $\geq 2.8 \times 10^{-4}$ and wind speed was less than 0.5 m s^{-1} . In addition, molecular diffusion could play an important role for HONO uptake on the surface, especially when the winds speed is larger than $\sim 1 \text{ m s}^{-1}$. Regarding the uptake of NO_2 on the ground surface, the range of NO_2 uptake coefficients as 2.4×10^{-7} to 3.5×10^{-6} obtained in the present
505 work indicates limitation only by the reactive uptake process. The consistency between our findings and the values of these parameters in models (Wong et al., 2011; Zhang et al., 2016) suggest that the broad scale applicability of these field-derived terms for surface conversion of NO_2 should therefore be possible. However, those value of γ found for HONO ($\gamma_{\text{HONO, ground}} = 1.7 \times 10^{-5}$ to 2.8×10^{-4}) require further exploration from various field environments and
510 controlled lab studies.

4.3 Daytime HONO

HONO concentrations started to increase after sunrise and peaked at 7:00 (UTC) (Figure 4), during that time it also underwent photolysis, eventually reaching a steady state between 10:30–16:30 (UTC). Throughout the day, HONO was observed to reach an averaged
515 minimum mixing ratio of 98 ± 15 pptv (10:30-16:30 UTC). Since NO and NO_2 have not the same diurnal cycle as HONO (Figure 4), the reactions 2 and 3a are not expected to be responsible for this HONO morning peak, but could be the main HONO source for period of 10:30-16:30 (UTC). Hence, three hypotheses (section 3.3) would be proposed to explain the observed diurnal variations, including that dew droplets on ground surfaces serve as a sink of
520 HONO during the night and become a morning source by releasing the trapped HONO back into ambient air, and others are photochemical processes such as reactions 3b and 6.

4.3.1 Photostationary state in the gas phase

The measured diurnal daytime HONO could be compared to model results by assuming an instantaneous photo-equilibrium between the gas-phase formation (reaction 3a) and gas-phase
525 loss processes (reactions 1 and 9), which is described by the following expression (Kleffmann et al., 2005):

$$[\text{HONO}]_{pss} = \frac{k_{3a}[\text{OH}][\text{NO}]}{J_{\text{HONO}} + k_9[\text{OH}]} \quad (\text{Eq. 8})$$

OH concentration was estimated from linear function of the global radiation flux vs. OH

radical concentration as described in the previous section and shown in **Figure 6b**, J_{HONO} was
 530 calculated using TUV model as described in section 2.6. The rate constants of NO+OH (k_{3a})
 and HONO+OH (k_9) are referred to $7.4 \times 10^{-12} \text{ cm}^3 \text{ molecule}^{-1} \text{ s}^{-1}$ (Burkholder et al., 2015) and
 $6.0 \times 10^{-12} \text{ cm}^3 \text{ molecule}^{-1} \text{ s}^{-1}$ (Atkinson et al., 2004), respectively. As a result, shown in **Figure**
6b, the $[\text{HONO}]_{\text{pss}}$ (violet curve) could not explain the sudden HONO increase after sunrise
 535 concentration. However, some studies (Michoud et al., 2012; Sörgel et al., 2011) already
 discussed that the stationary state of HONO can be only reached during noontime. Hence, a
 model calculation (named Model 1) was also used to discuss the HONO contribution from the
 gas-phase reaction of NO with OH radical.

$$\frac{d[\text{HONO}]}{dt} = k_{3a}[\text{OH}][\text{NO}] + k_{\text{het}}[\text{NO}_2] - J_{\text{HONO}}[\text{HONO}] - k_9[\text{HONO}][\text{OH}] \quad (\text{Eq. 9})$$

540 k_{het} derived from this work is 0.027 h^{-1} , $[\text{NO}]$ and $[\text{NO}_2]$ are averaged concentrations
 from this field measurement as shown in **Figure 6a**. The results are shown in **Figure 6b**
 (orange line). It is reasonable to indicate that the reaction 3a only contribute 30-55% to the
 HONO increase in the early morning (4:30-7:30 UTC). **Reaction 3a can continually**
contribute 50% of the measured HONO from 10:30 to 16:30 (UTC). However, regarding on
 545 **the large uncertainty of [OH] but also large variability of HONO mixing ratio, the “unknown**
HONO sources” could be not crucial but it could be exist due to the observation of Figure 6.
Basically, the additional HONO contribution rate could be estimated from following equation:

$$P_{\text{unknown}} = \frac{d[\text{HONO}]}{dt} + J_{\text{HONO}}[\text{HONO}] + k_9[\text{OH}][\text{HONO}] - k_{3a}[\text{OH}][\text{NO}] \quad (\text{Eq. 10})$$

550 **However,** an additional source of $91 \pm 41 \text{ pptv h}^{-1}$ was derived beside OH reaction with NO
 according to a HONO mixing ratio $98 \pm 15 \text{ pptv}$ for the time period of 10:30 to 16:30 (UTC).
This could be well explained by the photochemical processes such as reactions 3b and 6 and
would be discussed deeply in the next section.

4.3.2 Evidence for nighttime deposited HONO as a morning source

As observed in our field measurement and shown in Figure 2, the HONO concentrations
 555 always presented a strong increase from 4:00 – 7:00 (UTC). Which induces three hypotheses:
 (a) photolysis of gas-phase and particulate nitrate, (b) photosensitized conversion of NO_2 , (c)
 dew on ground surfaces served as HONO sink during the night and become a morning source
 by releasing the trapped nitrite back into ambient air.

To identify this HONO source, the chemical box model as expressed in equation 11 was
 560 **extended** with additional processes. Heterogeneous reaction of NO_2 on the wet surface
 (reaction 2) and HONO deposition on the ground surface were firstly used to quantify the
 contributions of the well-known HONO production and loss processes. In addition, the
 HONO deposition on the ground surface independent on RH (24 hours, named Model 2) and

its dependence on RH (nighttime 17:00-8:00 UTC, named Model 3) are also discussed.

$$565 \quad \frac{d[HONO]}{dt} = k_{3a}[OH][NO] + k_{het}[NO_2] - J_{HONO}[HONO] - k_9[HONO][OH] - \frac{1}{4}\gamma_{HONO,ground}[HONO]\frac{v_{HONO,ground}}{H} \quad (\text{Eq. 11})$$

Both the surface production of HONO through NO₂ heterogeneous reaction and subsequent loss by ground surface deposition are already termed in equation 4 and 7, respectively. The mixing layer height H was calculated from the backward trajectory based on GDAS data as shown in Figure S7 and dynamic conditions of boundary layer height were used. Here, $k_{het} = 0.027 \text{ h}^{-1}$ and $\gamma_{HONO,ground} = (1.0 \pm 0.4) \times 10^{-4}$ that we calculated from our observations are applied to the model calculation to simulate the diurnal cycle of HONO. As shown in Figure 6, both Model 2 (blue line) and Model 3 (green square) cannot explain the HONO morning peak but Model 3 (green square) can well reproduce the nighttime HONO, indicating that surface loss of HONO is an important sink to consider when the RH was saturated. Hence, Model 3 was used as the basic run for the following model calculation.

To investigate the contribution of photolysis of nitric acid and nitrate (HNO₃/NO₃⁻) (reaction 6) on the diurnal HONO based on the hypothesis (a), the following model calculation (Model 4) was made:

$$580 \quad \frac{d[HONO]}{dt} = k_{3a}[OH][NO] + k_{het}[NO_2] + J_{HNO_3}[HNO_3/NO_3^-] - J_{HONO}[HONO] - k_9[HONO][OH] - \frac{1}{4}\gamma_{HONO,ground}[HONO]\frac{v_{HONO,ground}}{H} \quad (\text{Eq. 12})$$

Here gas-phase HNO₃ and particle NO₃⁻ are summed up and the photolysis frequency J_{HNO_3} was derived from the TUV model by multiplying an enhanced factor of 30 due to a faster photolysis of particle-phase HNO₃ (Romer et al., 2018). As a result, the photolysis of HNO₃/NO₃⁻ (Model 4, pink line) could not reproduce the HONO morning peak shown in Figure 6. However, it could well reproduce the HONO for the time period of 10:30 to 16:30 (UTC).

To investigate the contribution of photosensitized conversion of NO₂ (reaction 3b) on the diurnal HONO based on the second hypothesis, the following model calculation (Model 5) was performed:

$$590 \quad \frac{d[HONO]}{dt} = k_{3a}[OH][NO] + k_{het}[NO_2] + \frac{1}{4}(\gamma_a \frac{S_a}{V} + \gamma_g \frac{S_g}{V})v_{NO_2}J_{NO_2}[NO_2] - J_{HONO}[HONO] - k_9[HONO][OH] - \frac{1}{4}\gamma_{HONO,ground}[HONO]\frac{v_{HONO,ground}}{H} \quad (\text{Eq. 13})$$

Here the γ_a and γ_g are the light-enhanced NO₂ uptake coefficient of 2.5×10^{-4} and 2.0×10^{-5} (Stemmler et al., 2006) on the aerosol surface and ground surface, respectively. And J_{NO_2} was multiplied with $\frac{\text{light intensity}}{400}$ when the light intensity $\geq 400 \text{ W m}^{-2}$. As shown in Figure 6

(Model 5, cyan line), the photosensitized NO₂ on the aerosol and ground surface could not reproduce the HONO morning peak. This favors the third hypothesis that dew evaporation processes release HONO resulting in the sudden morning peak.

Indeed, as shown in Figure S10, the HONO morning peak always happens according to a fast decrease of RH between 4:30-9:00 (UTC). However, there is one case happened at 1:00 (UTC) on April 25th, 2018, possibly due to an upcoming strong wind which decreased the RH and evaporated the dew water on the ground surface. It should be noted that this HONO morning peak was never observed during this field measurement period without a fast RH decrease, in case of **dry ground surface** as it was observed during the morning of April 23rd, 2018. To figure out the relationship between temporary HONO emission from dew water and decreasing RH, the following equation was defined:

$$k_{\text{emission}} = \frac{d\left(\frac{\text{HONO}_{\text{unknown}}}{99.5-\text{RH}}\right)}{dt} \quad (\text{Eq. 14})$$

where HONO_{unknown} = HONO_{measure} – HONO_{Model4} was calculated for each day in the whole campaign period. Then k_{emission} could be obtained from the linear least square analysis of $\frac{\text{HONO}_{\text{unknown}}}{99.5-\text{RH}}$ vs. the internal time of HONO morning peak (4:30-7:00, UTC) as shown in Figure 7. Then the maximum and minimum of k_{emission} are obtained as 0.026±0.008 and 0.006±0.001 pptv %⁻¹ s⁻¹, respectively, with an average of 0.016±0.014 pptv %⁻¹ s⁻¹ as presented in Table 4. The average value was used in the following model calculation to reproduce the diurnal cycle of HONO.

$$\begin{aligned} \frac{d[\text{HONO}]}{dt} = & k_{3a}[\text{OH}][\text{NO}] + k_{\text{het}}[\text{NO}_2] + J_{\text{HNO}_3}[\text{HNO}_3/\text{NO}_3^-] + \frac{1}{4}(\gamma_a \frac{S_a}{V} + \gamma_g \frac{S_g}{V})v_{\text{NO}_2} J_{\text{NO}_2}[\text{NO}_2] + \\ & k_{\text{emission}}*(99.5-\text{RH}) - J_{\text{HONO}}[\text{HONO}] - k_9[\text{HONO}][\text{OH}] - \\ & \frac{1}{4}\gamma_{\text{HONO,ground}}[\text{HONO}]\frac{v_{\text{HONO,ground}}}{H} \end{aligned} \quad (\text{Eq. 15})$$

The Model 6 (red line) result in Figure 6b shows that HONO deposited to the ground surface at night could represent the HONO morning peak. In Figure S11, the observed HONO atmospheric mixing ratio and the calculated HONO mixing ratio by model 6 using a minimum dew HONO emission $k_{\text{emission}} = 0.006$ pptv %⁻¹ s⁻¹ and maximum dew HONO emission $k_{\text{emission}} = 0.026$ pptv %⁻¹ s⁻¹, respectively, show that HONO emission from the dew water evaporation was at least 90% and likely in excess of 100% of the calculated unknown HONO morning peak, which may continually serve as HONO source for the whole daytime depending on the weather condition, for example at cloudy days.

4.3.3 HONO emission from dew water evaporation in the morning

The hypothetical morning HONO mixing ratio (pptv) due to the complete dew water evaporation could be estimated from the following equation by taking the measured dew

nitrite and the mixing layer height:

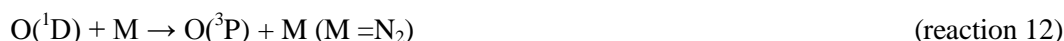
$$630 \quad [\text{HONO}] = \frac{2 \times \text{LAI} \times F_{\text{NO}_2}}{\text{mixing height}} \quad (\text{Eq. 16})$$

F_{NO_2} is the NO_2 concentration per m^2 of the glass sampler surface. During the HONO peak at 6 or 7 UTC, the mixing height was 175-600 m explored by meteorological data (GDAS-data) and the mixing height ranged from 20 m to 200 m at 0:00 – 5:00 UTC. Regarding the grass height during the dew measurements (~30cm) that is approximately the height in April 2018 and May 2019, we used a factor of 6 for LAI. Hence, the morning HONO mixing ratio could be estimated as: 2264.1 ± 612.3, 1132.1 ± 306.2, 452.8 ± 122.5, 226.4 ± 61.2 and 75.5 ± 20.4 pptv, respectively, for a mixing height of 20, 40, 100, 200 and 600 m using the mean F_{NO_2} from May 11th 2019 for the calculation. It shows that the HONO mixing ratio within 40 m mixing height is similar with the measured HONO morning peak of 1400 ± 100 pptv (section 4.3), which was able to detect by MARGA and LOPAP as both inlets were within this layer.

Indeed, few field studies (He et al., 2006; Rubio et al., 2009) have reported that dew water can serve as a sink and a temporary reservoir of atmospheric HONO. Previously, the role of dew as a nighttime reservoir and morning source for atmospheric NH_3 has been reported by Wentworth et al. (2016). Our results suggest that nocturnally deposited HONO forms a ground surface reservoir, which can be released in the following morning by dew evaporation. Therefore, a significant fraction of the daytime HONO source can be explained for the Melpitz observations.

4.3.4 Impact on the primary OH sources

HONO serves as an important primary source of OH during daytime in the troposphere (Kleffmann et al., 2005; Villena et al., 2011; Kanaya et al., 2007) and Seiler et al. (2012) reported that the HONO is almost the only source of OH radicals in the early morning. The morning peak of HONO is mainly released from the dew evaporation and could imply a strong supply of OH radicals and hence enhances atmospheric oxidizing capacity in the atmosphere around Melpitz. Here, the net rate of OH radical from the HONO photolysis was calculated and compared with that from ozone photolysis, which is typically proposed as the major OH radical source in the atmosphere where water vapor is not limiting.



Other OH sources, such as photolysis of oxidized VOCs, peroxides and ozonolysis of unsaturated VOCs are not considered due to the lack of measurement data for these radical precursors. The net rate of OH production from HONO photolysis (P_{HONO}) was calculated by the source strength subtracting the sink terms due to reactions 3a and 9. The OH production

rate (P_{O_3}) from O_3 photolysis can be calculated by using the method proposed by Su et al. (2008) and (Li et al., 2018).

$$P_{HONO} = J_{HONO}[HONO] - k_{3a}[NO][OH] - k_9[HONO][OH] \quad (\text{Eq.17})$$

$$P_{O_3} = 2J(O^1D)[O_3] \left(\frac{k_{12}[H_2O]}{k_{13}[M] + k_{12}[H_2O]} \right) \quad (\text{Eq. 18})$$

Where $J(O^1D)$ was obtained from the TUV model, the temperature dependence of k_{12} and k_{13} are taken from JPL/NASA Evaluation Number 18 (Burkholder et al., 2015). As shown in Figure 8, the photolysis of HONO produced similar amounts of OH compared with photolysis of ozone at the mean daytime (9:00-14:00, UTC), as $(7.2 \pm 2.0) \times 10^5$ molecule $\text{cm}^{-3} \text{s}^{-1}$. P_{O_3} was, as expected, highest during the highest J values and negligible at the sunrise and sunset. P_{HONO} had a similar trend after the noontime but presented a strong OH production around 7:00 (UTC) due to the HONO morning peak from the dew water evaporation process. These results demonstrate the significant role of HONO in the atmospheric oxidizing capacity, especially for areas that experience frequent dew formation. In addition, the OH concentration calculated from the global radiation flux measurement was also shown in yellow color of Figure 8. The different trend of calculated OH concentration compared with P_{HONO} indicate that the morning OH concentration could be highly underestimated.

5 Conclusion and Atmospheric Implications

The inter-comparison of MARGA and LOPAP for the HONO measurement was applied from April 19th to 29th, 2018 at the Melpitz site. Higher HONO mixing ratio (ca. 90%) were obtained from MARGA compared with that of LOPAP caused by heterogeneous reactions within the MARGA WRD or potential sampling inlet artefact. However, the diurnal cycles of HONO mixing ratio were captured by both instruments.

The dew water NO_2^- concentration per m^2 of glass sampler surface was determined to be 7.83–9.43 $\mu\text{g m}^{-2}$. Thus, the morning HONO mixing ratio depending on dew water evaporation could be calculated and ranged from 1234.1 \pm 161.9 to 41.1 \pm 5.4 pptv for mixing height of 20 to 600 m, respectively, assuming a homogeneous mixing of evaporated HONO.

Well-defined diurnal cycles of HONO with concentration peaks in the early morning and in the evening are found. High time resolution of HONO measurements revealed (i) the vehicle emission is a negligible HONO source at the Melpitz site; (ii) HONO formed from the heterogeneous reaction NO_2 on the ground surface is the dominant nighttime source with a high NO_2 -HONO conversion frequency of $0.027 \pm 0.017 \text{ h}^{-1}$; (iii) significant amounts of HONO (970 \pm 730 pptv) deposited to the ground surface at night. The accurate observations of HONO and NO_2 allowed direct evaluation of the ground uptake coefficients for these species at night: $\gamma_{\text{NO}_2 \rightarrow \text{HONO}_g} = 2.4 \times 10^{-7}$ to 3.5×10^{-6} , $\gamma_{\text{HONO}_{\text{ground}}} = 1.7 \times 10^{-5}$ to 2.8×10^{-4} . The ground uptake coefficient of NO_2 and HONO are within the ranges of laboratory and model

coefficients, and the range of HONO uptake coefficient values calculated in this investigation are potentially limited by a combination of transport and diffusion to the ground surface.

700

A chemical model utilizing observational constraints on the HONO chemical system based on known sources and sinks support the hypothesis that dew water on the ground surface, especially on leaf surfaces, behave as a sink at night and a temporary reservoir for atmospheric HONO in the morning. The dew evaporation had a negative relationship with the RH in the atmosphere and, hence, the HONO emission rate was estimated to be 0.016 ± 0.014 pptv %⁻¹ s⁻¹ dependent on the RH after sunrise (start from 4:00, UTC, during this campaign period). Furthermore, the formation and evaporation of dew on the ground surface influence significantly the air-surface exchange of HONO and, thus, its temporal distributions in the atmospheric boundary layer in the morning and night. The OH production rate from the photolysis of HONO compared with that from photolysis of O₃ showed that this dew emission of HONO can strongly enhance the OH reactivity throughout morning time and, hence, plays a vital role in the atmospheric oxidation.

705

710

Author contributions

RY wrote the paper with input from all authors. BS and GS analyzed the MARGA and dew data and wrote the paper. RY and BG conducted the HONO measurement using LOPAP. TT and AW were responsible for the particle measurement. AM and HH designed the experiments and lead the campaign. All co-authors commented on the manuscript.

720

Competing interests

The authors declare to have no competing interests.

Acknowledgements

The authors acknowledge financial support of this study and deployment of the MARGA system by the German Federal Environment Agency (UBA) research foundation under contracts No:351 01 093 and 351 01 070, as well as the European Union (EU) for the Transnational access (TNA) under ACTRIS-2: Comparison of HONO-measurements with MARGA and LOPAP at TROPOS research-site Melpitz (MARLO) is part of the project that has received funding from the European Union's Horizon 2020 research and innovation programme under grant agreement No 654109. For the laboratory analysis and the preparation of solutions, we thank A. Dietze, A. Rödger and S. Fuchs. For the support especially in the field, we thank R. Rabe and A. Grüner. We thank also the TROPOS mechanical workshop for the construction of the dew sampler. The CNRS team (Orléans-France) acknowledges the support from Labex Voltaire (ANR-10-LABX-100-01) and ARD PIVOTS program

730

735 (supported by the Centre-Val de Loire regional council). Europe invests in Centre-Val de Loire with the European Regional Development Fund.

References

- Acker, K., Spindler, G., and Brüggemann, E.: Nitrous and nitric acid measurements during the INTERCOMP2000 campaign in Melpitz, *Atmos. Environ.*, **38**, 6497-6505, 10.1016/j.atmosenv.2004.08.030, 2004.
- 740 Aliche, B., Platt, U., and Stutz, J.: Impact of nitrous acid photolysis on the total hydroxyl radical budget during the Limitation of Oxidant Production/Pianura Padana Produzione di Ozono study in Milan, *J. Geophys. Res. Atmos.*, **107**, 8196, doi:10.1029/2000JD000075, 2002.
- Aliche, B., Geyer, A., Hofzumahaus, A., Holland, F., Konrad, S., Pätz, H. W., Schäfer, J., Stutz, J., 745 Volz-Thomas, A., and Platt, U.: OH formation by HONO photolysis during the BERLIOZ experiment, *J. Geophys. Res. Atmos.*, **108**, 8247, doi:10.1029/2001JD000579, 2003.
- Ammann, M., Kalberer, M., Jost, D. T., Tobler, L., Rössler, E., Piguet, D., Gäggeler, H. W., and Baltensperger, U.: Heterogeneous production of nitrous acid on soot in polluted air masses, *Nature*, **395**, 157, 10.1038/25965, 1998.
- 750 Ammann, M., Rössler, E., Strekowski, R., and George, C.: Nitrogen dioxide multiphase chemistry: Uptake kinetics on aqueous solutions containing phenolic compounds, *Phys. Chem. Chem. Phys.*, **7**, 2513-2518, 10.1039/B501808K, 2005.
- Arens, F., Gutzwiller, L., Baltensperger, U., Gäggeler, H. W., and Ammann, M.: Heterogeneous Reaction of NO₂ on Diesel Soot Particles, *Environ. Sci. Technol.*, **35**, 2191-2199, 10.1021/es000207s, 2001.
- 755 Atkinson, R., Baulch, D. L., Cox, R. A., Crowley, J. N., Hampson, R. F., Hynes, R. G., Jenkin, M. E., Rossi, M. J., and Troe, J.: IUPAC Task Group on Atmospheric Chemical Kinetic Data Evaluation, *Atmos. Chem. Phys.*, **4**, 1461-1738, 2004.
- Aubin, D. G., and Abbatt, J. P. D.: Interaction of NO₂ with Hydrocarbon Soot: Focus on HONO Yield, Surface Modification, and Mechanism, *J. Phys. Chem. A*, **111**, 6263-6273, 10.1021/jp068884h, 760 2007.
- Bernard, F., Cazaunau, M., Gosselin, B., Zhou, B., Zheng, J., Liang, P., Zhang, Y. J., Ye, X. N., Daële, V., Mu, Y. J., Zhang, R. Y., Chen, J. M., and Mellouki, A.: Measurements of nitrous acid (HONO) in urban area of Shanghai, China, *Environmental Science and Pollution Research*, **23**, 5818-5829, 10.1007/s11356-015-5797-4, 2016.
- 765 Birmili, W., Stratmann, F., and Wiedensohler, A.: Design of a DMA-based size spectrometer for a large particle size range and stable operation, *J Aerosol Sci*, **30**, 549-553, 10.1016/S0021-8502(98)00047-0, 1999.
- Donaldson, M. A., Berke, A. E., and Raff, J. D.: Uptake of Gas Phase Nitrous Acid onto Boundary Layer Soil Surfaces, *Environ. Sci. Technol.*, **48**, 375-383, 10.1021/es404156a, 2014.
- 770 Febo, A., Perrino, C., and Cortiello, M.: A denuder technique for the measurement of nitrous acid in urban atmospheres, *Atmos. Environ.*, **27**, 1721-1728, 10.1016/0960-1686(93)90235-q, 1993.
- Finlayson-Pitts, B. J., Wingen, L. M., Sumner, A. L., Syomin, D., and Ramazan, K. A.: The heterogeneous hydrolysis of NO₂ in laboratory systems and in outdoor and indoor atmospheres: An integrated mechanism, *Phys. Chem. Chem. Phys.*, **5**, 223-242, 10.1039/B208564J, 2003.
- 775 Finlayson-Pitts, B. J.: Reactions at surfaces in the atmosphere: integration of experiments and theory as necessary (but not necessarily sufficient) for predicting the physical chemistry of aerosols, *Phys. Chem. Chem. Phys.*, **11**, 7760-7779, 10.1039/b906540g, 2009.
- Genfa, Z., Slanina, S., Boring, C. B., Jongejan, P. A. C., and Dasgupta, P. K.: Continuous wet denuder measurements of atmospheric nitric and nitrous acids during the 1999 Atlanta Supersite, *Atmos.*

- 780 Environ., 37, 1351-1364, 10.1016/S1352-2310(02)01011-7, 2003.
- Gerecke, A., Thielmann, A., Gutzwiller, L., and Rossi, M. J.: The chemical kinetics of HONO formation resulting from heterogeneous interaction of NO₂ with flame soot, *Geophysical Research Letters*, 25, 2453-2456, 10.1029/98gl01796, 1998.
- 785 Größ, J., Hamed, A., Sonntag, A., Spindler, G., Manninen, H. E., Nieminen, T., Kulmala, M., Hörrak, U., Plass-Dülmer, C., Wiedensohler, A., and Birmili, W.: Atmospheric new particle formation at the research station Melpitz, Germany: connection with gaseous precursors and meteorological parameters, *Atmos. Chem. Phys.*, 18, 1835-1861, 10.5194/acp-18-1835-2018, 2018.
- Gustafsson, R. J., Kyriakou, G., and Lambert, R. M.: The molecular mechanism of tropospheric nitrous acid production on mineral dust surfaces, *ChemPhysChem*, 9, 1390-1393, 790 10.1002/cphc.200800259, 2008.
- Gutzwiller, L., Arens, F., Baltensperger, U., Gäggeler, H. W., and Ammann, M.: Significance of Semivolatile Diesel Exhaust Organics for Secondary HONO Formation, *Environ. Sci. Technol.*, 36, 677-682, 10.1021/es015673b, 2002.
- 795 He, Y., Zhou, X., Hou, J., Gao, H., and Bertman, S. B.: Importance of dew in controlling the air-surface exchange of HONO in rural forested environments, *Geophys. Res. Lett.*, 33, doi:10.1029/2005GL024348, 2006.
- Heland, J., Kleffmann, J., Kurtenbach, R., and Wiesen, P.: A New Instrument To Measure Gaseous Nitrous Acid (HONO) in the Atmosphere, *Environ. Sci. Technol.*, 35, 3207-3212, 10.1021/es000303t, 2001.
- 800 Huang, G., Zhou, X. L., Deng, G. H., Qiao, H. C., and Civerolo, K.: Measurements of atmospheric nitrous acid and nitric acid, *Atmos. Environ.*, 36, 2225-2235, 10.1016/s1352-2310(02)00170-x, 2002.
- Huang, R. J., Yang, L., Cao, J. J., Wang, Q. Y., Tie, X. X., Ho, K. F., Shen, Z. X., Zhang, R. J., Li, G. H., Zhu, C. S., Zhang, N. N., Dai, W. T., Zhou, J. M., Liu, S. X., Chen, Y., Chen, J., and O'Dowd, C. D.: Concentration and sources of atmospheric nitrous acid (HONO) at an urban site in Western China, 805 *Sci. Total Environ.*, 593, 165-172, 10.1016/j.scitotenv.2017.02.166, 2017.
- Huff, A. K., and Abbatt, J. P. D.: Kinetics and Product Yields in the Heterogeneous Reactions of HOBr with Ice Surfaces Containing NaBr and NaCl, *J. Phys. Chem. A*, 106, 5279-5287, 10.1021/jp014296m, 2002.
- 810 Kalberer, M., Ammann, M., Arens, F., Gäggeler, H. W., and Baltensperger, U.: Heterogeneous formation of nitrous acid (HONO) on soot aerosol particles, *J. Geophys. Res. Atmos.*, 104, 13825-13832, doi:10.1029/1999JD900141, 1999.
- Kanaya, Y., Cao, R., Akimoto, H., Fukuda, M., Komazaki, Y., Yokouchi, Y., Koike, M., Tanimoto, H., Takegawa, N., and Kondo, Y.: Urban photochemistry in central Tokyo: 1. Observed and modeled OH and HO₂ radical concentrations during the winter and summer of 2004, *J. Geophys. Res. Atmos.*, 112, doi:10.1029/2007JD008670, 2007.
- 815 Kanda, Y., and Taira, M.: Chemiluminescent method for continuous monitoring of nitrous acid in ambient air, *Anal. Chem.*, 62, 2084-2087, 10.1021/ac00218a007, 1990.
- Kleffmann, J., Becker, K. H., and Wiesen, P.: Heterogeneous NO₂ conversion processes on acid surfaces: Possible atmospheric implications, *Atmos. Environ.*, 32, 2721-2729, 820 10.1016/s1352-2310(98)00065-x, 1998.
- Kleffmann, J., Gavriloaiei, T., Hofzumahaus, A., Holland, F., Koppmann, R., Rupp, L., Schlosser, E., Siese, M., and Wahner, A.: Daytime formation of nitrous acid: A major source of OH radicals in a forest, *Geophys. Res. Lett.*, 32, doi:10.1029/2005GL022524, 2005.

- 825 Kleffmann, J., Lörzer, J. C., Wiesen, P., Kern, C., Trick, S., Volkamer, R., Rodenas, M., and Wirtz, K.: Intercomparison of the DOAS and LOPAP techniques for the detection of nitrous acid (HONO), *Atmos. Environ.*, **40**, 3640-3652, <https://doi.org/10.1016/j.atmosenv.2006.03.027>, 2006.
- Kleffmann, J., and Wiesen, P.: Technical Note: Quantification of interferences of wet chemical HONO LOPAP measurements under simulated polar conditions, *Atmos. Chem. Phys.*, **8**, 6813-6822, 10.5194/acp-8-6813-2008, 2008.
- 830 Kurtenbach, R., Becker, K. H., Gomes, J. A. G., Kleffmann, J., Lörzer, J. C., Spittler, M., Wiesen, P., Ackermann, R., Geyer, A., and Platt, U.: Investigations of emissions and heterogeneous formation of HONO in a road traffic tunnel, *Atmos. Environ.*, **35**, 3385-3394, 10.1016/s1352-2310(01)00138-8, 2001.
- Lahoutifard, N., Ammann, M., Gutzwiller, L., Ervens, B., and George, C.: The impact of multiphase reactions of NO₂ with aromatics: a modelling approach, *Atmos. Chem. Phys.*, **2**, 215-226, 10.5194/acp-2-215-2002, 2002.
- 835 Lammel, G., and Perner, D.: The atmospheric aerosol as a source of nitrous acid in the polluted atmosphere, *J. Aerosol Sci.*, **19**, 1199-1202, [https://doi.org/10.1016/0021-8502\(88\)90135-8](https://doi.org/10.1016/0021-8502(88)90135-8), 1988.
- 840 Lammel, G., and Cape, J. N.: Nitrous acid and nitrite in the atmosphere, *Chem. Soc. Rev.*, **25**, 361-369, 10.1039/CS9962500361, 1996.
- Li, D., Xue, L., Wen, L., Wang, X., Chen, T., Mellouki, A., Chen, J., and Wang, W.: Characteristics and sources of nitrous acid in an urban atmosphere of northern China: Results from 1-yr continuous observations, *Atmos. Environ.*, **182**, 296-306, 10.1016/j.atmosenv.2018.03.033, 2018.
- 845 Li, G., Lei, W., Zavala, M., Volkamer, R., Dusanter, S., Stevens, P., and Molina, L. T.: Impacts of HONO sources on the photochemistry in Mexico City during the MCMA-2006/MILAGO Campaign, *Atmos. Chem. Phys.*, **10**, 6551-6567, 10.5194/acp-10-6551-2010, 2010.
- Li, X., Brauers, T., Häseler, R., Bohn, B., Fuchs, H., Hofzumahaus, A., Holland, F., Lou, S., Lu, K. D., Rohrer, F., Hu, M., Zeng, L. M., Zhang, Y. H., Garland, R. M., Su, H., Nowak, A., Wiedensohler, A., Takegawa, N., Shao, M., and Wahner, A.: Exploring the atmospheric chemistry of nitrous acid (HONO) at a rural site in Southern China, *Atmos. Chem. Phys.*, **12**, 1497-1513, 10.5194/acp-12-1497-2012, 2012.
- 850 Liu, X., Cheng, Y., Zhang, Y., Jung, J., Sugimoto, N., Chang, S.-Y., Kim, Y. J., Fan, S., and Zeng, L.: Influences of relative humidity and particle chemical composition on aerosol scattering properties during the 2006 PRD campaign, *Atmos. Environ.*, **42**, 1525-1536, <https://doi.org/10.1016/j.atmosenv.2007.10.077>, 2008.
- 855 Lu, K., Zhang, Y., Su, H., Brauers, T., Chou, C. C., Hofzumahaus, A., Liu, S. C., Kita, K., Kondo, Y., Shao, M., Wahner, A., Wang, J., Wang, X., and Zhu, T.: Oxidant (O₃ + NO₂) production processes and formation regimes in Beijing, *Journal of Geophysical Research: Atmospheres*, **115**, 10.1029/2009jd012714, 2010.
- 860 Michoud, V., Kukui, A., Camredon, M., Colomb, A., Borbon, A., Miet, K., Aumont, B., Beekmann, M., Durand-Jolibois, R., Perrier, S., Zapf, P., Siour, G., Ait-Helal, W., Locoge, N., Sauvage, S., Afif, C., Gros, V., Furger, M., Ancellet, G., and Doussin, J. F.: Radical budget analysis in a suburban European site during the MEGAPOLI summer field campaign, *Atmos. Chem. Phys.*, **12**, 11951-11974, 10.5194/acp-12-11951-2012, 2012.
- 865 Monge, M. E., D'Anna, B., Mazri, L., Giroir-Fendler, A., Ammann, M., Donaldson, D. J., and George, C.: Light changes the atmospheric reactivity of soot, *Proceedings of the National Academy of*

- Sciences, 107, 6605-6609, 10.1073/pnas.0908341107, 2010.
- 870 Pagsberg, P., Bjergbakke, E., Ratajczak, E., and Sillesen, A.: Kinetics of the gas phase reaction $\text{OH} + \text{NO}(+\text{M}) \rightarrow \text{HONO}(+\text{M})$ and the determination of the UV absorption cross sections of HONO, *Chem. Phys. Lett.*, 272, 383-390, [https://doi.org/10.1016/S0009-2614\(97\)00576-9](https://doi.org/10.1016/S0009-2614(97)00576-9), 1997.
- Pfeifer, S., Birmili, W., Schladitz, A., Müller, T., Nowak, A., and Wiedensohler, A.: A fast and easy-to-implement inversion algorithm for mobility particle size spectrometers considering particle number size distribution information outside of the detection range, *Atmos. Meas. Tech.*, 7, 95-105, 10.5194/amt-7-95-2014, 2014.
- 875 Platt, U., Perner, D., Harris, G. W., Winer, A. M., and Pitts, J. N.: Observations of nitrous acid in an urban atmosphere by differential optical absorption, *Nature*, 285, 312-314, 10.1038/285312a0, 1980.
- Romer, P. S., Wooldridge, P. J., Crouse, J. D., Kim, M. J., Wennberg, P. O., Dibb, J. E., Scheuer, E., Blake, 880 D. R., Meinardi, S., Brosius, A. L., Thames, A. B., Miller, D. O., Brune, W. H., Hall, S. R., Ryerson, T. B., and Cohen, R. C.: Constraints on Aerosol Nitrate Photolysis as a Potential Source of HONO and NO_x, *Environmental Science & Technology*, 52, 13738-13746, 10.1021/acs.est.8b03861, 2018.
- Rubio, M. A., Lissi, E., Villena, G., Elshorbany, Y. F., Kleffmann, J., Kurtenbach, R., and Wiesen, P.: Simultaneous measurements of formaldehyde and nitrous acid in dew and gas phase in the 885 atmosphere of Santiago, Chile, *Atmos. Environ.*, 43, 6106-6109, 10.1016/j.atmosenv.2009.09.017, 2009.
- Sörgel, M., Regelin, E., Bozem, H., Diesch, J.-M., Drewnick, F., Fischer, H., Harder, H., Held, A., Hosaynali-Beygi, Z., Martinez, M., and Zetzsch, C.: Quantification of the unknown HONO daytime source and its relation to NO₂, *Atmos. Chem. Phys.*, 11, 10433-10447, 890 10.5194/acp-11-10433-2011, 2011.
- Sarwar, G., Roselle, S. J., Mathur, R., Appel, W., Dennis, R. L., and Vogel, B.: A comparison of CMAQ HONO predictions with observations from the Northeast Oxidant and Particle Study, *Atmospheric Environment*, 42, 5760-5770, <https://doi.org/10.1016/j.atmosenv.2007.12.065>, 2008.
- Schiller, C. L., Locquiao, S., Johnson, T. J., and Harris, G. W.: Atmospheric measurements of HONO by 895 tunable diode laser absorption spectroscopy, *J. Atmos. Chem.*, 40, 275-293, 10.1023/a:1012264601306, 2001.
- Seiler, W., Becker, K.-H., and Schaller, E.: *Tropospheric Chemistry: Results of the German Tropospheric Chemistry Programme*, Springer Netherlands, 2012.
- Spindler, G., Hesper, J., Brüggemann, E., Dubois, R., Müller, T., and Herrmann, H.: Wet annular denuder 900 measurements of nitrous acid: laboratory study of the artefact reaction of NO₂ with S(IV) in aqueous solution and comparison with field measurements, *Atmos. Environ.*, 37, 2643-2662, 10.1016/s1352-2310(03)00209-7, 2003.
- Spindler, G., Müller, T., Brüggemann, E., Gnauk, T., and Herrmann, H.: Long-term size-segregated characterization of PM₁₀, PM_{2.5}, and PM₁ at the IfT research station Melpitz downwind of Leipzig 905 (Germany) using high and low-volume filter samplers, *Atmos. Environ.*, 38, 5333-5347, 10.1016/j.atmosenv.2003.12.047, 2004.
- Stemmler, K., Ammann, M., Donders, C., Kleffmann, J., and George, C.: Photosensitized reduction of nitrogen dioxide on humic acid as a source of nitrous acid, *Nature*, 440, 195, 10.1038/nature04603, 2006.
- 910 Stieger, B., Spindler, G., Fahlbusch, B., Müller, K., Grüner, A., Poulain, L., Thöni, L., Seitler, E., Wallasch, M., and Herrmann, H.: Measurements of PM₁₀ ions and trace gases with the online system

- MARGA at the research station Melpitz in Germany – A five-year study, *J. Atmos. Chem.*, 75, 33-70, 10.1007/s10874-017-9361-0, 2018.
- 915 Su, H., Cheng, Y. F., Shao, M., Gao, D. F., Yu, Z. Y., Zeng, L. M., Slanina, J., Zhang, Y. H., and Wiedensohler, A.: Nitrous acid (HONO) and its daytime sources at a rural site during the 2004 PRIDE-PRD experiment in China, *J. Geophys. Res. Atmos.*, 113, 10.1029/2007jd009060, 2008.
- Su, H., Cheng, Y. F., Oswald, R., Behrendt, T., Trebs, I., Meixner, F. X., Andreae, M. O., Cheng, P., Zhang, Y., and Poschl, U.: Soil Nitrite as a Source of Atmospheric HONO and OH Radicals, *Science*, 333, 1616-1618, 10.1126/science.1207687, 2011.
- 920 Tuch, T. M., Haudek, A., Müller, T., Nowak, A., Wex, H., and Wiedensohler, A.: Design and performance of an automatic regenerating adsorption aerosol dryer for continuous operation at monitoring sites, *Atmos. Meas. Tech.*, 2, 417-422, 10.5194/amt-2-417-2009, 2009.
- VandenBoer, T. C., Brown, S. S., Murphy, J. G., Keene, W. C., Young, C. J., Pszenny, A. A. P., Kim, S., Warneke, C., de Gouw, J. A., Maben, J. R., Wagner, N. L., Riedel, T. P., Thornton, J. A., Wolfe, D. E., 925 Dubé, W. P., Öztürk, F., Brock, C. A., Grossberg, N., Lefer, B., Lerner, B., Middlebrook, A. M., and Roberts, J. M.: Understanding the role of the ground surface in HONO vertical structure: High resolution vertical profiles during NACHTT-11, *J. Geophys. Res. Atmos.*, 118, 10.1029/2012jd018171, doi:10.1002/jgrd.50721, 2013.
- VandenBoer, T. C., Markovic, M. Z., Sanders, J. E., Ren, X., Pusede, S. E., Browne, E. C., Cohen, R. C., 930 Zhang, L., Thomas, J., Brune, W. H., and Murphy, J. G.: Evidence for a nitrous acid (HONO) reservoir at the ground surface in Bakersfield, CA, during CalNex 2010, *Journal of Geophysical Research: Atmospheres*, 119, 9093-9106, 10.1002/2013jd020971, 2014.
- VandenBoer, T. C., Young, C. J., Talukdar, R. K., Markovic, M. Z., Brown, S. S., Roberts, J. M., and Murphy, 935 J. G.: Nocturnal loss and daytime source of nitrous acid through reactive uptake and displacement, *Nature Geoscience*, 8, 55-60, 10.1038/ngeo2298, 2015.
- Villena, G., Wiesen, P., Cantrell, C. A., Flocke, F., Fried, A., Hall, S. R., Hornbrook, R. S., Knapp, D., Kosciuch, E., Mauldin III, R. L., McGrath, J. A., Montzka, D., Richter, D., Ullmann, K., Walega, J., Weibring, P., Weinheimer, A., Staebler, R. M., Liao, J., Huey, L. G., and Kleffmann, J.: Nitrous acid 940 (HONO) during polar spring in Barrow, Alaska: A net source of OH radicals?, *Journal of Geophysical Research-Atmospheres*, 116, 10.1029/2011jd016643, 2011.
- Wang, J., Zhang, X., Guo, J., Wang, Z., and Zhang, M.: Observation of nitrous acid (HONO) in Beijing, China: Seasonal variation, nocturnal formation and daytime budget, *Sci. Total Environ.*, 587, 350-359, 10.1016/j.scitotenv.2017.02.159, 2017.
- Wang, L. M., and Zhang, J. S.: Detection of nitrous acid by cavity ring down spectroscopy, *Environ. Sci. 945 Technol.*, 34, 4221-4227, 10.1021/es0011055, 2000.
- Wang, S., Zhou, R., Zhao, H., Wang, Z., Chen, L., and Zhou, B.: Long-term observation of atmospheric nitrous acid (HONO) and its implication to local NO₂ levels in Shanghai, China, *Atmos. Environ.*, 77, 718-724, 10.1016/j.atmosenv.2013.05.071, 2013.
- Wentworth, G. R., Murphy, J. G., Benedict, K. B., Bangs, E. J., and Collett Jr., J. L.: The role of dew as a 950 night-time reservoir and morning source for atmospheric ammonia, *Atmos. Chem. Phys.*, 16, 7435-7449, 10.5194/acp-16-7435-2016, 2016.
- Wiedensohler, A.: An approximation of the bipolar charge distribution for particles in the submicron size range, *J. Aerosol Sci.*, 19, 387-389, [https://doi.org/10.1016/0021-8502\(88\)90278-9](https://doi.org/10.1016/0021-8502(88)90278-9), 1988.
- Wiedensohler, A., Birmili, W., Nowak, A., Sonntag, A., Weinhold, K., Merkel, M., Wehner, B., Tuch, T., 955 Pfeifer, S., Fiebig, M., Fjåraa, A. M., Asmi, E., Sellegri, K., Depuy, R., Venzac, H., Villani, P., Laj, P.,

- 960 Aalto, P., Ogren, J. A., Swietlicki, E., Williams, P., Roldin, P., Quincey, P., Hüglin, C., Fierz-Schmidhauser, R., Gysel, M., Weingartner, E., Riccobono, F., Santos, S., Grüning, C., Faloon, K., Beddows, D., Harrison, R., Monahan, C., Jennings, S. G., O'Dowd, C. D., Marinoni, A., Horn, H.-G., Keck, L., Jiang, J., Scheckman, J., McMurry, P. H., Deng, Z., Zhao, C. S., Moerman, M., Henzing, B., de Leeuw, G., Löschau, G., and Bastian, S.: Mobility particle size spectrometers: harmonization of technical standards and data structure to facilitate high quality long-term observations of atmospheric particle number size distributions, *Atmos. Meas. Tech.*, 5, 657-685, 10.5194/amt-5-657-2012, 2012.
- 965 Wiedensohler, A., Wiesner, A., Weinhold, K., Birmili, W., Hermann, M., Merkel, M., Müller, T., Pfeifer, S., Schmidt, A., Tuch, T., Velarde, F., Quincey, P., Seeger, S., and Nowak, A.: Mobility particle size spectrometers: Calibration procedures and measurement uncertainties, *Aerosol Sci. Technol.*, 52, 146-164, 10.1080/02786826.2017.1387229, 2018.
- 970 Wohlfahrt, G., Sapinsky, S., Tappeiner, U., and Cernusca, A.: Estimation of plant area index of grasslands from measurements of canopy radiation profiles, *Agric. For. Meteorol.*, 109, 1-12, [https://doi.org/10.1016/S0168-1923\(01\)00259-3](https://doi.org/10.1016/S0168-1923(01)00259-3), 2001.
- Wong, K. W., Oh, H.-J., Lefer, B. L., Rappenglück, B., and Stutz, J.: Vertical profiles of nitrous acid in the nocturnal urban atmosphere of Houston, TX, *Atmos. Chem. Phys.*, 11, 3595-3609, 10.5194/acp-11-3595-2011, 2011.
- 975 Xu, Z., Liu, Y., Nie, W., Sun, P., Chi, X., and Ding, A.: Evaluating the measurement interference of wet rotating-denuder-ion chromatography in measuring atmospheric HONO in a highly polluted area, *Atmos. Meas. Tech.*, 12, 6737-6748, 10.5194/amt-12-6737-2019, 2019.
- Ye, C., Gao, H., Zhang, N., and Zhou, X.: Photolysis of Nitric Acid and Nitrate on Natural and Artificial Surfaces, *Environ. Sci. Technol.*, 50, 3530-3536, 10.1021/acs.est.5b05032, 2016.
- 980 Yu, Y., Galle, B., Panday, A., Hodson, E., Prinn, R., and Wang, S.: Observations of high rates of NO₂-HONO conversion in the nocturnal atmospheric boundary layer in Kathmandu, Nepal, *Atmos. Chem. Phys.*, 9, 6401-6415, 10.5194/acp-9-6401-2009, 2009.
- Zhang, B., and Tao, F.-M.: Direct homogeneous nucleation of NO₂, H₂O, and NH₃ for the production of ammonium nitrate particles and HONO gas, *Chem. Phys. Lett.*, 489, 143-147, 10.1016/j.cplett.2010.02.059, 2010.
- 985 Zhang, L., Wang, T., Zhang, Q., Zheng, J., Xu, Z., and Lv, M.: Potential sources of nitrous acid (HONO) and their impacts on ozone: A WRF-Chem study in a polluted subtropical region, *J. Geophys. Res. Atmos.*, 121, 3645-3662, doi:10.1002/2015JD024468, 2016.
- Zhou, X., Gao, H., He, Y., Huang, G., Bertman, S. B., Civerolo, K., and Schwab, J.: Nitric acid photolysis on surfaces in low-NO_x environments: Significant atmospheric implications, *Geophys. Res. Lett.*, 30, 10.1029/2003gl018620, 2003.
- 990 Zhou, X., Huang, G., Civerolo, K., Roychowdhury, U., and Demerjian, K. L.: Summertime observations of HONO, HCHO, and O₃ at the summit of Whiteface Mountain, New York, *J. Geophys. Res. Atmos.*, 112, doi:10.1029/2006JD007256, 2007.
- 995 Zhou, X., Zhang, N., TerAvest, M., Tang, D., Hou, J., Bertman, S., Alaghmand, M., Shepson, P. B., Carroll, M. A., Griffith, S., Dusanter, S., and Stevens, P. S.: Nitric acid photolysis on forest canopy surface as a source for tropospheric nitrous acid, *Nature Geoscience*, 4, 440-443, 10.1038/ngeo1164, 2011.

Table 1. Mean and mean error as 2 times the standard deviation of the measured HONO (LOPAP) and the other pollutants in the Melpitz station during daytime (D, 04:00-18:00, UTC) and nighttime (N, 18:00-04:00, UTC).

	D	N		D	N
NO (ppbv)	1.0±0.5	0.5±0.3	HCl (ppbv) ^b	0.02±0.03	0.01±0.01
NO _x (ppbv)	4±1	6±2	HNO ₃ (ppbv) ^b	0.2±0.1	0.2±0.1
NO ₂ (ppbv)	3±1	5±2	NH ₃ (ppbv) ^b	17±7	8±4
HONO (pptv) ^a	162±96	254±114	Cl ⁻ (µg m ⁻³) ^b	0.03±0.04	0.01±0.01
O ₃ (ppbv)	36±7	19±13	NO ₃ ⁻ (µg m ⁻³) ^b	3±2	2±1
SO ₂ (ppbv)	0.8±0.4	0.5±0.3	SO ₄ ²⁻ (µg m ⁻³) ^b	1.4±0.5	1.3±0.6
T (°C)	16±3	11±5	Na ⁺ (µg m ⁻³) ^b	0.02±0.03	0.01±0.01
RH (%)	67±7	85±11	NH ₄ ⁺ (µg m ⁻³) ^b	1.1±0.7	0.8±0.4
Wind speed (m s ⁻¹)	3±2	1.2±0.7	K ⁺ (µg m ⁻³) ^b	0	0.001±0.002
HONO/NO _x (%)	0.04±0.02	0.05±0.02	Mg ²⁺ (µg m ⁻³) ^b	0.03±0.01	0.02±0.04
NO/NO _x (%)	0.3±0.1	0.1±0.1	Ca ²⁺ (µg m ⁻³) ^b	0.2±0.1	0.2±0.1
OH (molecule cm ⁻³)	(2.8±0.7)×10 ⁶		NO ₂ ⁻ (µg m ⁻³) ^b	0.01±0.01	0.03±0.02

^a HONO derived from LOPAP;

^b data obtained from the MARGA instrument

Table 2. Nitrite concentration measured in dew water.

Date	Plate	Initial hour	Final hour	Volume (ml)	Blank NO ₂ ⁻	Final NO ₂ ⁻	F _{NO2-}	pH
2019	number	(UTC)	(UTC)		(µg L ⁻¹)	(µg L ⁻¹) ^a	(µg m ⁻²)	
8/5	1	18:00	5:25	76.60	0.0018	41.87	2.10	6.40
	2		5:45	75.60	0.0017	42.84	2.20	6.45
11/5	1	18:00	3:20	94.00	0.0055	128.23	8.00	7.00
	2		4:20	80.00	0.0005	120.43	6.40	6.90
	1	3:30	5:20	13.00	0.0006	164.62	1.43	7.00
13/5	1	18:00	4:45	72.00	0.0001	43.87	2.10	6.30
	2		5:20	79.00	0.0001	58.81	3.10	6.40
14/5	1	18:00	5:00	15.00	0.0001	148.90	1.50	6.80
	2		5:00	21.00	0.0001	91.44	1.30	6.70

^a Final NO₂⁻ = Raw NO₂⁻ - Blank NO₂⁻

^b pH was measured by a pH meter on a subsample of the total volume

Table 3. The ratio HONO/NO₂ and the NO₂-HONO conversion frequency during nighttime.

Date	UTC	R ₂	HONO/NO ₂	k _{het} (h ⁻¹)
19/04/2018	17:30-19:50	0.45	0.118±0.010	0.043±0.002
21/04/2018	18:20-20:30	0.64	0.055±0.004	0.012±0.002
22/04/2018	18:10-21:20	0.79	0.161±0.005	0.030±0.002
25/04/2018	17:31-21:20	0.69	0.061±0.003	0.010±0.001
27/04/2018	18:00-23:41	0.48	0.113±0.006	0.016±0.001
28/04/2018	18:00-19:50	0.44	0.152±0.008	0.050±0.004
			0.110±0.041	0.027±0.017

Table 4. Summary of the temporary HONO emission rate from dew water, k_{emission} from April 19th to 29th, 2018.

Period	k_{emission} (pptv % ⁻¹ s ⁻¹)	
	Min	Max
2018/4/21	0.0054	0.0357
2018/4/22	0.0048	0.0314
2018/4/24	0.0057	0.0192
2018/4/26	0.0067	0.0302
2018/4/27	0.0048	0.0215
2018/4/28	0.0079	0.017
Average	0.006±0.001	0.026±0.008

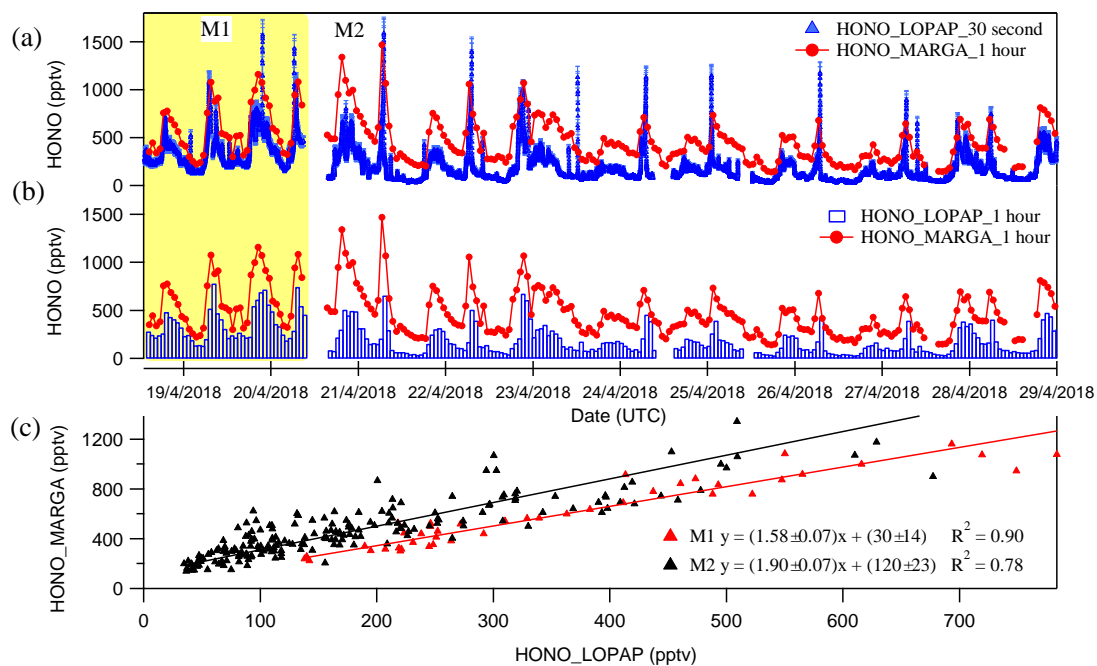


Figure 1. Time courses of HONO as hourly measured by MARGA and 30 seconds measured by LOPAP (a) and normalized hourly for LOPAP (b). (c) represents the orthogonal regression analysis between MARGA and LOPAP dependent on two different comparison period (M1 and M2).

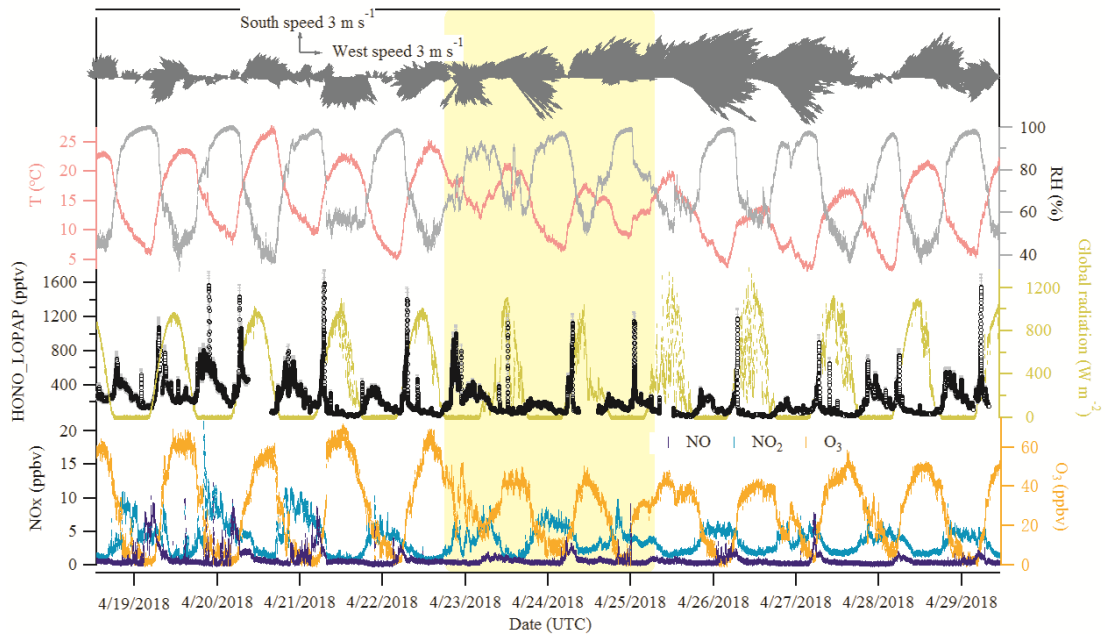


Figure 2. Time series of HONO (LOPAP measurement), NO, NO₂, O₃, global radiation, temperature (T), relative humidity (RH) and surface wind in Melpitz from April 19th to 29th, 2018. The **gaps were** mainly due to the maintenance of the instruments. The yellow shadow indicates **two sets of observations** discussed in section 3.3.

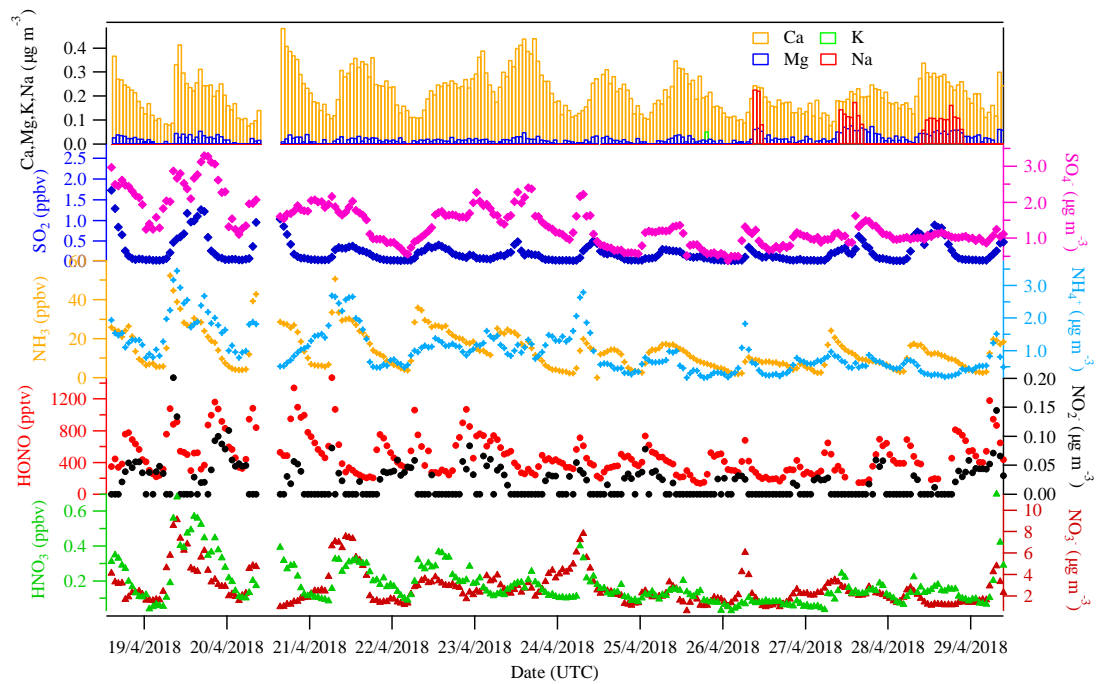


Figure 3. The hourly time-resolved quantification of water-soluble ions in PM_{10} (NO_3^- , SO_4^{2-} , NO_2^- , NH_4^+ , Na^+ , K^+ , Mg^{2+} , Ca^{2+}) and their corresponding trace gases (HONO, HNO_3 , SO_2 , NH_3) were measured by MARGA in Melpitz from April 19th to 29th, 2018.

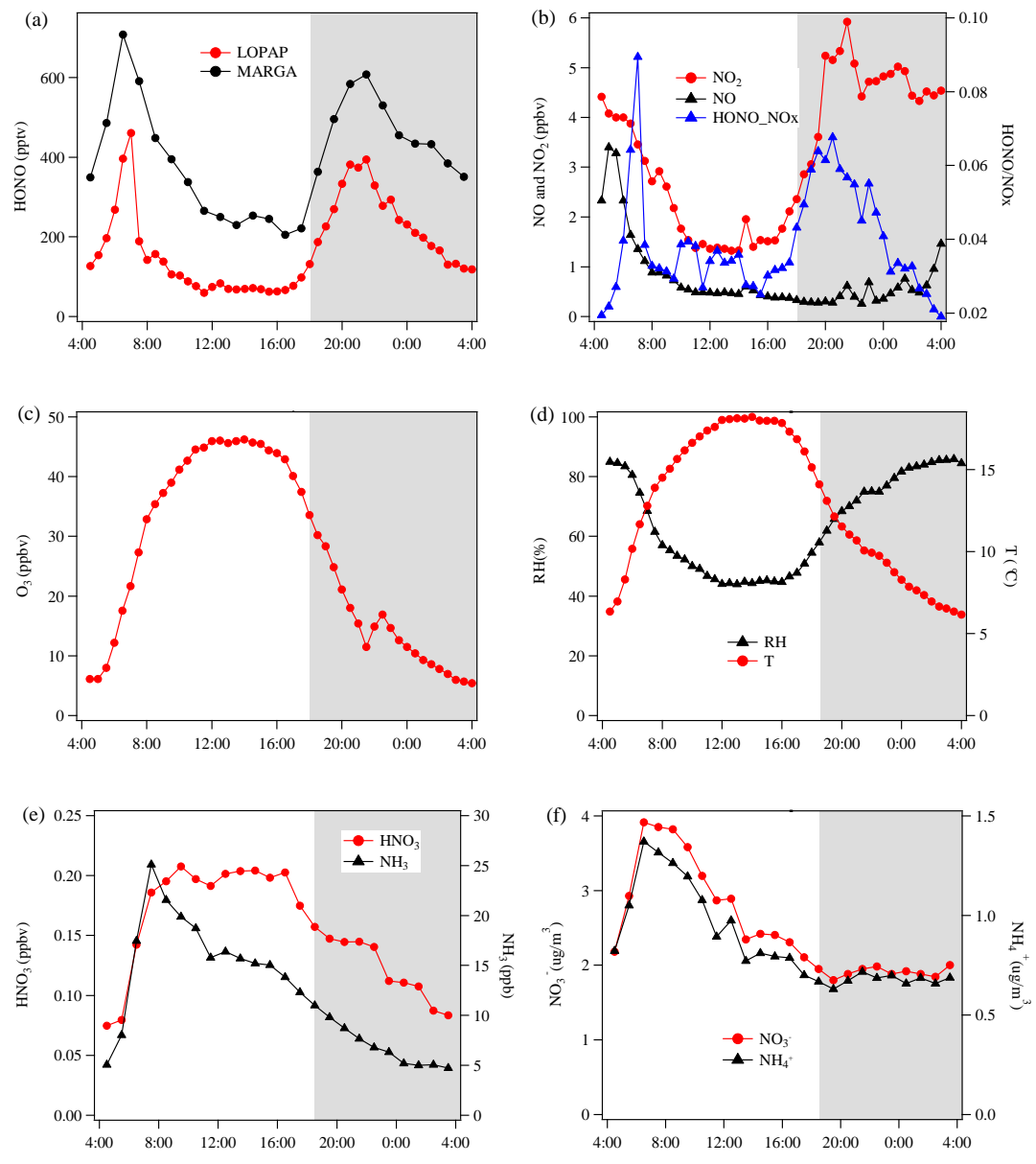


Figure 4. Diurnal variations of HONO and related species during the measurement period at Melpitz site. The grey shaded area indicates the nighttime period (18:00-04:00 UTC).

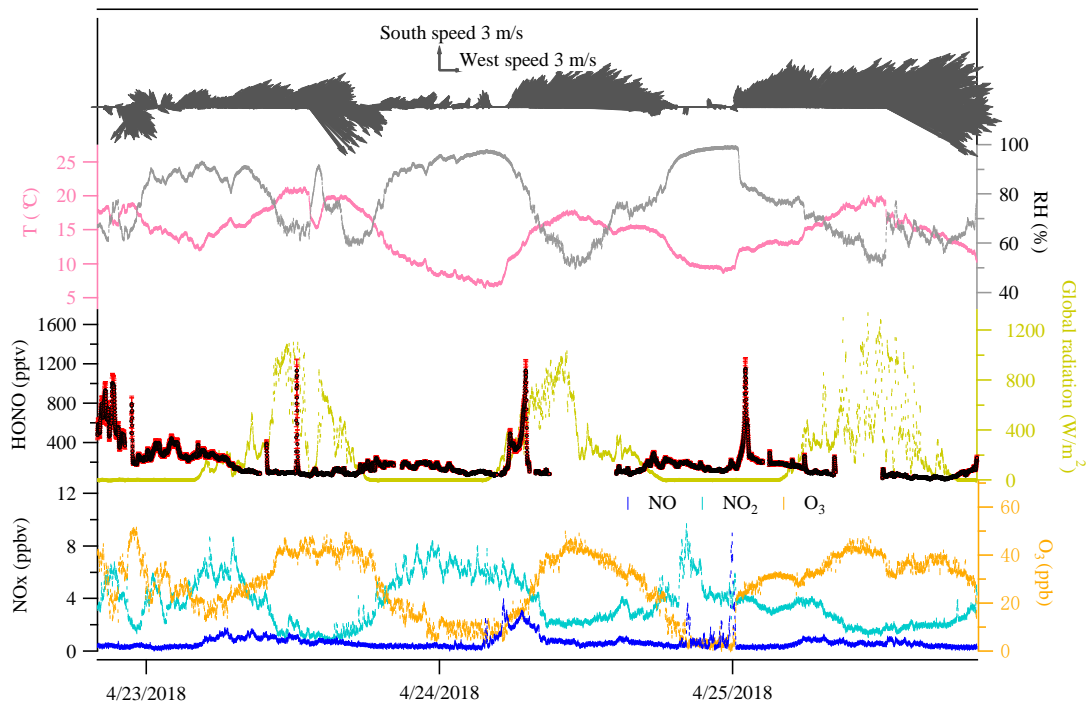


Figure 5. Case events for HONO (LOPAP) and related species at Melpitz site during the day April 23rd to 25th, 2018. The red color in the HONO panel indicates the measurement error of HONO concentrations.

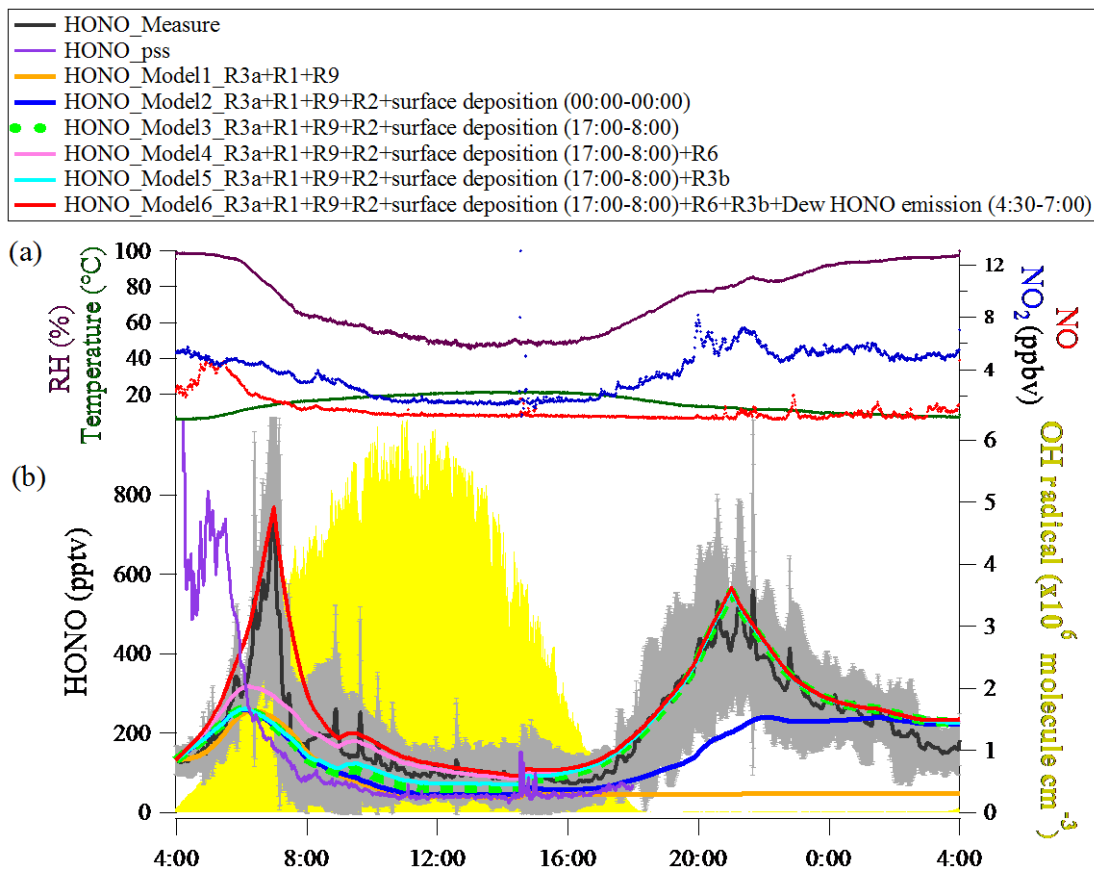


Figure 6. (a) Chemical Box model input values of measured constraints (averaged data) from April 19th to 29th, 2018 for diurnal modeling of HONO chemical behavior and quantifying the missing HONO source/sink. (b) Observed average HONO atmospheric concentration (black line, $\pm 1\sigma$ in shaded area) and the model calculated HONO concentration including different HONO production and loss processes. **Note:** R3a according to reaction 3a, R1 according to reaction 1, R9 according to reaction 9, R2 according to reaction 2, R6 according to reaction 6 and R3b according to reaction 3b in Table 1.

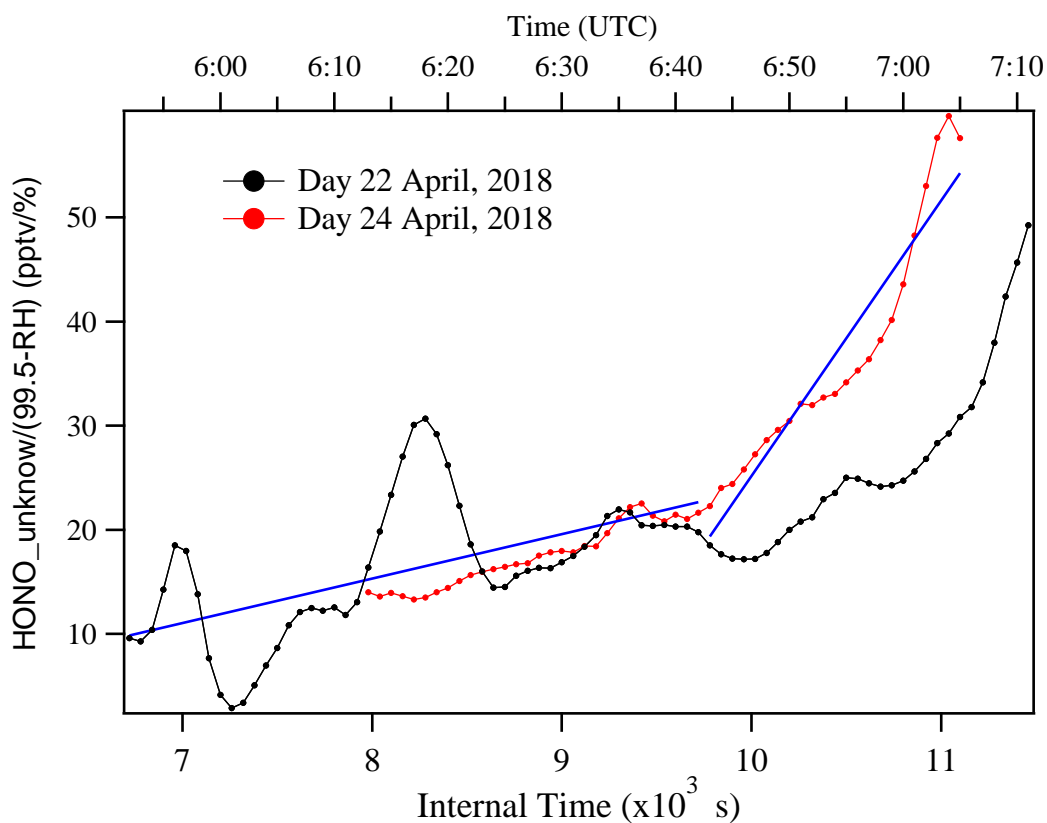


Figure 7. Example of $\frac{HONO_{unknown}}{99.5-RH}$ as a function of the internal time of HONO morning peak (zero point from time 4:30, UTC) to estimate the temporary HONO emission rate from dew water, $k_{emission}$. Blue line is the linear least-square analysis of $\frac{HONO_{unknown}}{99.5-RH}$ vs. internal time to obtain the minimum and maximum of $k_{emission}$, respectively.

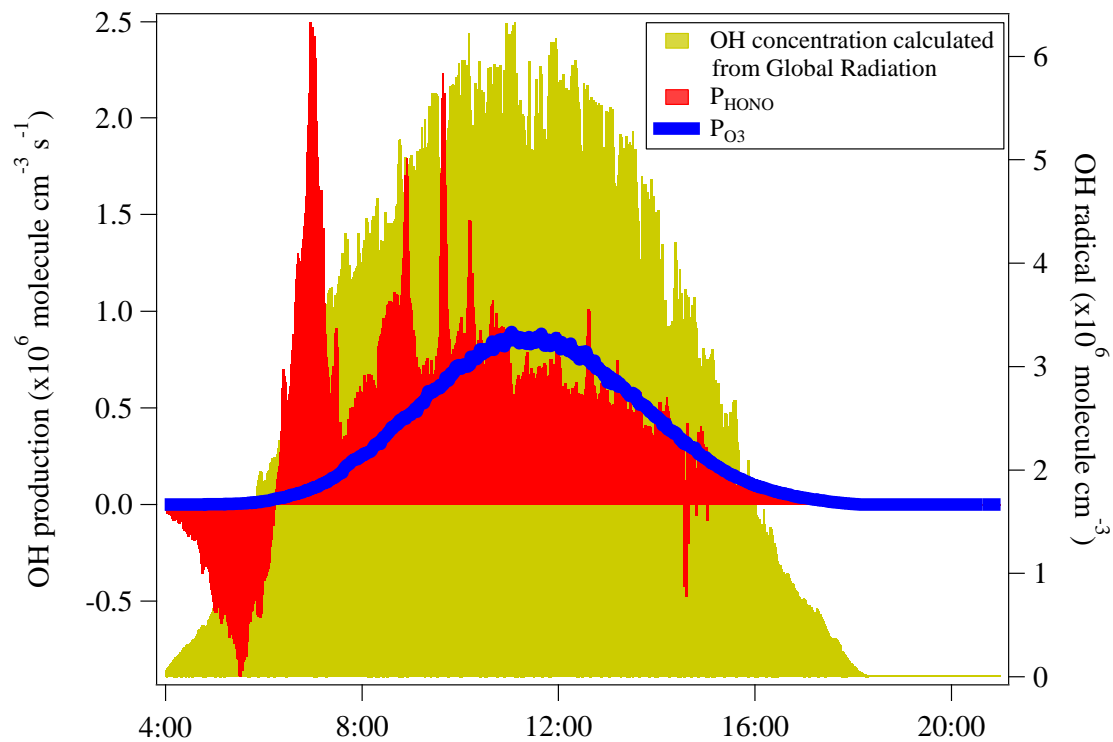


Figure 8. The OH production rates from photolysis of HONO and O₃ in Melpitz station from April 19th to 29th, 2018. The OH concentration is also shown as yellow area plot, which was calculated from the global radiation flux measurement: [OH]=A*Rad taken from Größ et al. (2018).